J. Fluid Mech. (2014), *vol.* 756, *pp.* 54–88.
doi:10.1017/jfm.2014.271

Segregation in dense sheared flows: gravity, temperature gradients, and stress partitioning

K. M. Hill[1,2,†] **and Danielle S. Tan**[1,‡]

[1]St Anthony Falls Laboratory, University of Minnesota, 2 Third Avenue SE, Minneapolis, MN 55414, USA

[2]Department of Civil Engineering, University of Minnesota, 500 Pillsbury Drive SE, Minneapolis, MN 55455, USA

(Received 27 July 2013; revised 10 March 2014; accepted 13 May 2014; first published online 1 September 2014)

It is well-known that in a dense, gravity-driven flow, large particles typically rise to the top relative to smaller equal-density particles. In dense flows, this has historically been attributed to gravity alone. However, recently kinetic stress gradients have been shown to segregate large particles to regions with higher granular temperature, in contrast to sparse energetic granular mixtures where the large particles segregate to regions with lower granular temperature. We present a segregation theory for dense gravity-driven granular flows that explicitly accounts for the effects of both gravity and kinetic stress gradients involving a separate partitioning of contact and kinetic stresses among the mixture constituents. We use discrete-element-method (DEM) simulations of different-sized particles in a rotated drum to validate the model and determine diffusion, drag, and stress partition coefficients. The model and simulations together indicate, surprisingly, that gravity-driven kinetic sieving is not active in these flows. Rather, a gradient in kinetic stress is the key segregation driving mechanism, while gravity plays primarily an implicit role through the kinetic stress gradients. Finally, we demonstrate that this framework captures the experimentally observed segregation reversal of larger particles downward in particle mixtures where the larger particles are sufficiently denser than their smaller counterparts.

Key words: granular media, mixing, multiphase and particle-laden flows

1. Introduction

Sheared mixtures of different-sized particles segregate into a wide range of segregation patterns, the complexity of which often defies the apparent simplicity of the conditions under which they occur: from relatively simple experimental flows in a shear cell (May *et al.* 2010*a*; May, Shearer & Daniels 2010*b*), in an inclined plane flow (Savage & Lun 1988; Gray & Thornton 2005; Gray & Chugunov 2006), and in a rotated drum (Hill, Caprihan & Kakalios 1997; Khakhar, McCarthy & Ottino 1997; Hill *et al.* 1999; Shinbrot & Muzzio 2000; Taberlet, Losert & Richard 2004),

†Email address for correspondence: kmhill@umn.edu

‡Present address: Department of Mechanical Engineering, National University of Singapore, 9 Engineering Dr. 1, Singapore 117575, Republic of Singapore.

to relatively complex geophysical flows in a riverbed (Dietrich *et al.* 1989; Paola & Seal 1995) and in a debris flow (Stock & Dietrich 2006; Hsu, Dietrich & Sklar 2008; Yohannes *et al.* 2010). The details of the segregation dynamics depend on several factors. Gravity has long been known to drive sorting of different types of particles (depending on relative size, density, etc.) (Donald & Roseman 1962; Bridgwater 1976; Williams 1976). Other mixture kinematics are important as well, such as gradients in granular temperature (i.e. the random kinetic energy of the particles) (Jenkins & Mancini 1987; Xu, Louge & Reeves 2003; Galvin, Dahl & Hrenya 2005), similar to gradients in kinetic stress (Fan & Hill 2011*b*), and solid fraction gradients (Hill & Fan 2008). Even the average solid volume fraction of the mixture can be significant: in a sparse sheared mixture of different-sized particles, the smaller particles move along a granular temperature gradient to regions of higher granular temperature; while in a dense sheared flow, the smaller particles segregate to regions of lower granular temperature (Fan & Hill 2011*a*,*b*). When segregation dynamics combine with other system details such as advection and diffusion (e.g. Hill *et al.* 1999), the segregation patterns that emerge can be even more complex. We focus here on the dynamics associated with the unmixing of particles in dense sheared gravity-driven flows, applicable to a wide range of systems of variable boundary conditions and advective flow patterns.

Much work has been done using kinetic theory (e.g. Jenkins & Mancini 1987; Xu *et al.* 2003; Galvin *et al.* 2005) to explain/predict segregation in sparse flows as the behaviour varies with particle size and density and kinematics such as granular temperature gradients. Unfortunately, in dense sheared flows enduring contacts and longer-range forces limit the applicability of kinetic theory. There is not yet an analogous physics-based framework for predicting segregation in dense sheared flows, although significant efforts have been made in extending kinetic theory to denser granular flows (Arnarson & Jenkins 2000, 2004; Galvin *et al.* 2005; Larcher & Jenkins 2009*a*,*b*, 2010, 2013). In this paper we focus on segregation in dense gravity-driven flows of different-sized particles with equal material density where, upon shearing, the large particles are often found at the top of the mixture.

The focus of modelling efforts of segregation in denser gravity-driven flows has been largely associated with gravity as the driving force. In most cases, large particles in the granular mixtures will rise in the opposite direction to gravity, toward a free surface in gravity-driven flows, while small particles sink. This phenomenon is often referred to as 'reverse grading' in certain geophysical problems (e.g. Middleton & Hampton 1976; Naylor 1980; Hill, DellAngelo & Meerschaert 2010*a*; Yohannes *et al.* 2010). Several mechanisms have been proposed for gravity-driven segregation of high solid fractions of different-sized particles (e.g. Savage & Lun 1988; Alonso, Satoh & Miyanami 1991; Dolgunin & Ukolov 1995; Gray & Thornton 2005; Gray & Chugunov 2006).

Historically, this size-dependent segregation is often associated with two simultaneous processes dubbed by Savage & Lun (1988) as 'kinetic sieving' and 'squeeze expulsion'. Essentially, gravity pushes all particles in one direction, but the structure associated with the high packing fraction prevents most particles from responding. Statistically, in a mixture of different-sized particles it is more likely that small particles will find holes sufficiently large for them to enter. As the mixture is excited and the particles shift, holes of different sizes open and close, giving the small particles opportunities to drop downward via what is referred to as a 'kinetic sieving' mechanism. A higher shear rate results in a more frequent availability of holes and thus a higher segregation rate. Mass balance is achieved when the

downward-migrating smaller particles squeeze the larger particles upward via Savage & Lun (1988)'s 'squeeze expulsion' mechanism. Savage & Lun (1988) developed a detailed statistical model to predict segregation trends based on this process.

More recently, Gray & Thornton (2005) and Gray & Chugunov (2006) have developed a continuum framework for this process based in part on mixture theory (which they later expanded into a theory incorporating multiple particle sizes (Gray & Ancey 2011)). In this model, the focus of the segregation mechanism is on the gradient in 'lithostatic pressure' induced by gravity. Thus, the model has the advantage of explicitly including gravity in the framework, although reference to an explicit dependence of segregation on shear rate is eliminated. The segregation mechanism is represented by the partitioning of pressure among the different species. The constituent which bears more of the stress relative to its local concentration moves to lower lithostatic pressures and the other constituent moves to higher pressures. With some assumptions about the pressure partitioning for a flowing bidisperse mixture, uniform in all directions but y, the segregation flux and segregation evolution equations take the form:

$$\phi^i\left(v^i - v\right) = \phi^i\left(1-\phi^i\right)q + \left[-D\frac{\partial \phi^i}{\partial y}\right], \tag{1.1a}$$

$$\frac{\partial \phi^i}{\partial t} + \frac{\partial}{\partial y}\left(\phi^i\left(v^i + \left(1-\phi^i\right)q\right)\right) + \left[-\frac{\partial}{\partial y}D\frac{\partial \phi^i}{\partial y}\right] = 0, \tag{1.1b}$$

$$q = A\frac{\mathrm{d}p}{\mathrm{d}y}. \tag{1.1c}$$

In these equations ϕ^i and v^i are the concentration and normal velocity of constituent i; v is the normal velocity of the mixture; D is a diffusion coefficient; q represents a maximum segregation velocity where $\mathrm{d}p/\mathrm{d}y$ is a pressure gradient associated with gravity and A contains some information about the stress partitioning and a linear drag coefficient. The bracketed terms involving diffusion were added to the original Gray & Thornton (2005) work by Gray & Chugunov (2006). For the purpose of the mathematical development in those papers, A and D were assumed constant. This framework has been shown to be effective in reproducing segregation trends in simple and complex granular flows by, for example, Wiederseiner *et al.* (2011), Thornton *et al.* (2012) and Weinhart, Luding & Thornton (2013). However those studies have also provided evidence that some details are not fully captured by the model.

Subsequent work has suggested specific modifications to this general framework to better capture the discrepancies between model and data. May *et al.* (2010*a*,*b*) considered the effects of a non-constant shear rate on the Gray–Thornton–Chugunov model in the form of a shear-rate-dependent maximal segregation rate $A(\mathrm{d}p/\mathrm{d}y) \propto \dot{\gamma}$ and found that the model captured features of mixing and segregation in an experimental shear cell. Marks & Einav (2011) showed that such a shear-rate-dependent form of the Gray–Thornton–Chugunov segregation model captured segregation well in a gravity-driven system modelled with a cellular automaton model. Weinhart *et al.* (2013) demonstrated that the linear drag law contained within A of the original Gray–Thornton–Chugunov framework may not be sufficient for capturing the drag in the system, which appeared to vary with time. Marks, Rognon & Einav (2012) derived an alternative form for the segregation term, $\phi^i(1-\phi^i)A(\mathrm{d}p/\mathrm{d}y)$ in (1.1*a*) and (1.1*b*). They partitioned the stresses explicitly according to particle size ratio; they derived a shear-rate-dependent segregation velocity, and they extended the

model to continuously varying particle size distributions. They demonstrated that their new model captured segregation dynamics in a simulated polydisperse mixture.

As effective as the framework captured by (1.1*a*) and (1.1*b*) is at representing segregation of large particles upward, it is limited to representing cases where the segregation magnitude and the relative segregation direction is known *a priori*. Recent variations (e.g. those of May *et al.* 2010*a*,*b*; Marks & Einav 2011; Marks *et al.* 2012) allow for variation of magnitude of segregation, but without consideration of how shear rate gradients might affect the direction of segregation. The magnitude of shear rate appears in some models for segregation in dense sheared granular flows (e.g. Savage & Lun 1988; May *et al.* 2010*a*,*b*; Marks & Einav 2011; Marks *et al.* 2012). However, it only mediates the rate at which segregation occurs. The effects of shear rate gradients on the segregation direction have generally not been considered in segregation models for dense systems. There are cases in which large particles (of density greater than or equal to the smaller particles) sink in dense sheared flows (e.g. Williams 1963; Félix & Thomas 2004; Jain, Ottino & Lueptow 2005; Hill *et al.* 2010*b*). In some of these cases, the large particles segregate to some intermediate height in a mixture, i.e. they sink partway in a mixture, depending on their initial location (e.g. Félix & Thomas 2004; Jain *et al.* 2005; Hill *et al.* 2010*b*). We hypothesize that this 'tunable' segregation is associated with certain flow dynamics acting simultaneously with gravity, specifically those associated with shear rate gradients.

Recently, we demonstrated that dynamics associated with shear rate gradients can also drive segregation in dense sheared systems (Fan & Hill 2011*a*,*b*). Specifically, in a vertical chute with roughened walls, large particles tend to segregate along shear rate gradients toward regions of highest shear rate and highest granular temperature (velocity fluctuations). This is consistent with early results of Stephens & Bridgwater (1978) and Foo & Bridgwater (1983). However, the segregation trends contrast with results from many authors (e.g. Leighton & Acrivos 1987*a*,*b*; Abbott *et al.* 1991, Krishnan, Beimfohr & Leighton 1996; Conway, Liu & Glasser 2006) on segregation in sparser dry granular systems and suspensions, in which large particles segregate to regions of lowest shear rate and lowest granular temperature. In this vertical chute configuration, gravity is acting in the direction normal to the segregation so it plays no direct role in the segregation process.

We recently developed a hydrodynamic model for shear-induced segregation of mixtures of different-sized particles in dense sheared flow (Fan & Hill 2011*b*). Specifically, we showed how gradients in kinetic stresses that arise from a shear rate gradient in combination with a kinetic sieving mechanism will segregate large particles to regions of high granular temperatures and small particles away from them. This model for shear-induced segregation is complementary to that of gravity-driven segregation developed by Gray & Thornton (2005), Gray & Chugunov (2006). The models represent different phenomena that coexist in many systems, particularly those of free-surface gravity-driven flow commonly used to investigate segregation effects in granular mixtures. The model in Fan & Hill (2011*b*) shows that the kinetic stress mechanism can affect the direction of segregation. The results motivate the question as to how the two sets of mechanisms – those associated with gravity and those associated with a shear rate gradient – work together in a system where both gravity and shear rates may simultaneously drive segregation in a dense granular system.

In this paper we address this question and provide a more complete model of segregation in dense gravity-driven granular flows. Specifically, we consider segregation of particles in flows where both pressure gradients induced by gravity and

kinetic stress gradients induced by a non-uniform shear rate coexist in the direction of segregation. In § 2, we present our theory and show how the addition of gravity to the model in Fan & Hill (2011*b*) changes the form of predicted segregation fluxes. In § 3, we present the basic details of the discrete-element-method (DEM) that simulations we use to investigate the theory applied to particles segregating in a rotated drum. In § 4, we present kinematics and dynamics in five different simulated granular mixtures in a rotated drum and in doing so, summarize the details the model should capture. Then, in §§ 5 and 6, we investigate the results from the different mixtures to validate the model and to understand what dynamics drives segregation differences from one mixture to the next. In particular, in § 5 we derive the stress partition coefficients as they vary with mixture concentration. In § 6, we first use the simulations to obtain drag and diffusion coefficients for our mixtures and compare them with analogous coefficients in related work, and we then compare model predictions with simulation results for all five mixtures throughout the segregation process. In § 7 we consider the generalization of this theory to other systems and other mixtures, and some next steps that are needed for further improving the model. In the last section, we present our conclusions with some directions for future work.

2. Theory

In this section we briefly outline our theoretical model for the segregating effects of gravity and shear rate gradients in dense gravity-driven sheared flows. Our model concerns binary mixtures of different-sized spherical particles with the same material density ρ_m. We denote bulk Eulerian properties of each species with superscripts and those of the mixture of both species together as variables without superscript. For example, we represent the local volume fraction filled with particles of species i by f^i; therefore, the local bulk mass density of species i, $\rho^i = \rho_m f^i$. We denote the concentration of species i by $\phi^i \equiv f^i/f$ which satisfies $\sum \phi^i = 1$. The average local density of the mixture $\rho = \sum \rho^i$ and the average local velocity $\boldsymbol{u} = \sum \boldsymbol{u}^i \phi^i$.

2.1. *Conservation equations for gravity-driven mixtures*

We first consider conservation of mass and momentum for the mixture when subjected to gravity:

$$\frac{\partial \rho}{\partial t} + \boldsymbol{\nabla} \cdot (\rho \boldsymbol{u}) = 0, \tag{2.1}$$

$$\frac{\partial}{\partial t}(\rho \boldsymbol{u}) + \boldsymbol{\nabla} \cdot (\rho \boldsymbol{u} \otimes \boldsymbol{u}) = \boldsymbol{\nabla} \cdot \boldsymbol{\sigma} + \boldsymbol{F}. \tag{2.2}$$

Here, $\boldsymbol{\sigma}$ represents the stress tensor, and $\boldsymbol{F}$ represents body forces. Since our mixture is subjected to gravity, $\boldsymbol{F} = \rho \boldsymbol{g}$, where $\boldsymbol{g}$ is the gravitational acceleration vector.

We consider systems in which the mixture kinematics reach steady state long before segregation and set $\partial \rho/\partial t, \partial(\rho \boldsymbol{u})/\partial t = 0$. We perform 'Reynolds decomposition' (Schlichting 1979) and set each variable q at position $\boldsymbol{r}$ equal to a sum of the local temporal average $\overline{\xi}(\boldsymbol{r})$ and the difference between its instantaneous and average values $\xi'(\boldsymbol{r}, t) = \xi(\boldsymbol{r}, t) - \overline{\xi}$. Considering this, we rewrite the momentum equation (2.2) for the j-direction as

$$\sum_k \frac{\partial}{\partial x_k} \left[(\overline{\rho} + \rho')(\overline{u}_j + u_j')(\overline{u}_k + u_k') \right] = \sum_k \frac{\partial}{\partial x_k} (\overline{\sigma}_{jk} + \sigma_{jk}') + \overline{F}_j + F_j'. \tag{2.3}$$

Here, $\overline{F}_j + F'_j = \overline{\rho} g_j + \rho' g_j$. We average the results in the context of relatively simple pseudo-two-dimensional systems such as in an inclined chute flow or in the centre of the thin flowing layer of granular materials rotated in a narrow drum. The average flow is primarily in one direction, the x-direction; the flow is nearly uniform in the x- and z-directions; and segregation occurs primarily in the third direction, the y-direction. The average flow direction is inclined at an angle θ to the horizontal, so that $g_y = g\cos\theta$, where $g = |\boldsymbol{g}|$. We take the average of both sides of (2.3), and assume that temporal correlations between velocity fluctuations and densities are negligible, i.e. $(\partial/\partial x_k)(\overline{u}_j\overline{\rho' u'_k})$, $(\partial/\partial x_k)(\overline{u}_k\overline{\rho' u'_j})$, $(\partial/\partial x_k)(\overline{\rho' u'_k u'_j}) \approx 0$. Then conservation of momentum, (2.3), in the y-direction may be simply expressed by:

$$\frac{\partial \rho\overline{v'v'}}{\partial y} = \frac{\partial \overline{\sigma}_{yy}}{\partial y} + \overline{\rho} g\cos\theta. \tag{2.4}$$

In this equation, $-\rho\overline{v'v'}$ is often referred to as a Reynolds stress component (Schlichting 1979; Campbell 2002), though we follow Chikkadi & Alam (2009) in their use of the term in the context of granular flows and denote $\overline{\sigma}^k_{yy} = \rho\overline{v'v'}$ as a kinetic stress, superscript k denoting 'kinetic'. We also note that for dry macroscopic particles, the normal contact stress will be solely compressive, whereas in the standard sign convention for $\boldsymbol{\sigma}$ (e.g. Batchelor 1967) positive normal stresses such as $\overline{\sigma}_{yy}$ are positive only for tensile, and negative for compressive stresses. We therefore define a contact stress tensor $\boldsymbol{\sigma}^c = -\boldsymbol{\sigma}$, superscript c denoting 'contact', so that terms such as $\overline{\sigma}^c_{yy}$ are positive for our problem. Then we rewrite (2.4) as:

$$\frac{\partial \overline{\sigma}^c_{yy}}{\partial y} + \frac{\partial \overline{\sigma}^k_{yy}}{\partial y} = \overline{\rho} g\cos\theta \tag{2.5}$$

which indicates that the sum of the gradients in contact and kinetic stresses supports the normalized weight of the particles.

2.2. *Conservation of mass and momentum for species in a mixture*

Next, we derive the conservation laws for each of the two species in the mixture using much of the notation from mixture theory (e.g. by Morland 1972, 1978, 1992):

$$\frac{\partial \rho^i}{\partial t} + \boldsymbol{\nabla}\cdot(\rho^i \boldsymbol{u}^i) = 0, \tag{2.6}$$

$$\frac{\partial(\rho^i \boldsymbol{u}^i)}{\partial t} + \boldsymbol{\nabla}\cdot(\rho^i \boldsymbol{u}^i \otimes \boldsymbol{u}^i) = \boldsymbol{\nabla}\cdot(\boldsymbol{\sigma}^i) + \boldsymbol{F}^i + \boldsymbol{\beta}^i. \tag{2.7}$$

Here, all of the terms used for species i are identical in form to those used for the mixture in (2.2), with the exception of the new term $\boldsymbol{\beta}^i$, which represents the interaction force exerted on species i by the other species; $\boldsymbol{\sigma}^i$ is the local stress borne by species i, and the total stress $\boldsymbol{\sigma} = \sum \boldsymbol{\sigma}^i$. By performing Reynolds decomposition and then averaging both sides of (2.7) we may rewrite (2.7) in the y-direction as

$$\frac{\partial \overline{\sigma}^{c,i}_{yy}}{\partial y} + \frac{\partial \overline{\sigma}^{k,i}_{yy}}{\partial y} = \overline{\beta}^i_y + \rho^i g\cos\theta. \tag{2.8}$$

Since all terms in (2.5) and (2.8) are averaged, from this point on we drop the overbar, so that unless noted otherwise, for each variable, ξ refers to the average $\overline{\xi}$.

We follow the suggestion of Gray & Thornton (2005), Gray & Chugunov (2006) and allow for the partitioning of both kinetic and contact stresses between the large and small particles to deviate from their concentrations, i.e. $\sigma_{yy}^{c,i} \neq \phi^i \sigma_{yy}^c$ and $\sigma_{yy}^{k,i} \neq \phi^i \sigma_{yy}^k$. Instead:

$$\sigma_{yy}^{c,i} = \psi^{c,i} \sigma_{yy}^c \quad \text{and} \quad \sigma_{yy}^{k,i} = \psi^{k,i} \sigma_{yy}^k, \tag{2.9a,b}$$

where we explicitly define the normal contact and kinetic stress partition coefficients as $\psi^{c,i}$ and $\psi^{k,i}$ respectively. Here, $\psi^{c,i}$ and $\psi^{k,i}$ are not necessarily equal to ϕ^i, nor equal to one another. To ensure that $\sum_i \sigma_{yy}^{c,i} = \sigma_{yy}^c$ and $\sum_i \sigma_{yy}^{k,i} = \sigma_{yy}^k$ two constraints must be satisfied: (i) that $\psi^L + \psi^S = 1$ (here, and from this point forward, superscripts S and L refer to quantities associated with the small and large particles, respectively), and (ii) if only one species is present then it must support the entire local stress, so that when $\phi^i = 1$, $\psi^{c,j} = \psi^{k,j} = \delta_{ij}$, where δ_{ij} is the Kronecker delta function. Otherwise, we do not specify a functional form for either and investigate their calculated values in our DEM simulations in § 3.2.

For the interaction term β_y^i, we propose a similar form to that proposed by Gray & Chugunov (2006) for granular mixtures and for flow through porous media provided by Morland (1992):

$$\beta_y^i = \sigma_{yy}^c \frac{\partial}{\partial y} \psi^{c,i} + \sigma_{yy}^k \frac{\partial}{\partial y} \psi^{k,i} - \rho^i c_D (v^i - v) - \rho d \frac{\partial \phi^i}{\partial y}. \tag{2.10}$$

The first two terms on the right-hand side of the equation ensure that the kinetic sieving processes are driven by intrinsic rather than partial stress gradients. The third term is effectively a linear drag law, where c_D is the linear drag coefficient. The fourth term acts as a 'remixing force' along gradients in the concentration of each species, where d is analogous to a linear diffusion coefficient.

Combining (2.8)–(2.10) with (2.5), we can express a normalized form of the segregation flux of species i, $\Phi_T^i \equiv \phi^i (v^i - v)$, as:

$$\Phi_T^i \equiv [\phi^i (v^i - v)]_T = \Phi_{\sigma k}^i + \Phi_g^i + \Phi_d^i, \tag{2.11}$$

where

$$\Phi_{\sigma k}^i = \frac{(\psi^{c,i} - \psi^{k,i})}{c_D} \frac{1}{\rho} \frac{\partial \sigma_{yy}^k}{\partial y}, \tag{2.12a}$$

$$\Phi_g^i = \frac{(\phi^i - \psi^{c,i})}{c_D} g \cos\theta, \tag{2.12b}$$

$$\Phi_d^i = -\frac{d}{c_D} \frac{\partial \phi^i}{\partial y}. \tag{2.12c}$$

This expression for the flux suggests that there are three 'forces' dictating the segregation behaviour. The first is controlled by the gradient in the kinetic stress of the mixture and the difference between the two stress partition coefficients. For a qualitative picture of the segregation process dictated by this term, we consider that the kinetic stress scales similarly to the granular temperature (e.g. Fan & Hill 2011*b*). A constituent that bears more kinetic stress might be considered more mobile and more likely to find spaces or vacancies to move away from the high-temperature region, somewhat like 'kinetic sieving' of the particles to the cooler region. On the other hand, a constituent that bears more contact stress is physically pushed

by interparticle contacts to a region of lower contact stress and higher temperature, somewhat like 'squeeze expulsion' in the qualitative balance of movement induced by kinetic sieving suggested by Savage & Lun (1988).

The second term in (2.11) is the mechanism associated with gravity, specifically the pressure gradient induced by gravity. If a species supports a higher fraction of the contact stress than its local concentration, the species moves in the direction opposite to gravity, toward the free surface. A physical picture of the segregation effect associated with this term might most easily be envisioned for systems where the kinetic stress is minimal. In this case, normal contact stress in the mixture should be approximately equal to the lithostatic pressure that increases with distance from the free surface, so each particle experiences a normal stress (or pressure) that increases with distance from the free surface. If this stress is equally partitioned among constituents, the pressure gradient exactly balances the weight of the particles and there is no segregation associated with this term. However, if one constituent supports a higher percentage of the normal stress than its concentration in the mixture, the stress gradient in the direction normal to the free surface across each particle in that species will push it upward. Similarly, if one species supports a lower percentage of the normal stress, the weight will not be balanced by the gradient in normal stress and it will sink. This term is closest to the segregation term in the model developed by Gray & Thornton (2005) and Gray & Chugunov (2006).

The third term in (2.11) is akin to a diffusion force. It is significant only when there is a concentration gradient of that species. Like normal Fickian diffusion with diffusion coefficient d/c_D, this term results in a segregation flux in the direction opposite to that of the concentration gradient of a particular species, and thus serves to limit the degree of local segregation.

Equation (2.11) is similar to that which Gray and colleagues derived for binary mixtures with a couple key differences. Specifically, in Gray & Chugunov (2006) the equivalent form would read:

$$\phi^i(v^i - v) = \frac{\phi^i - \psi^{p,i}}{c_D} g\cos\theta - \frac{d}{c_D}\frac{\partial \phi^i}{\partial y}, \tag{2.13}$$

where $\psi^{p,i}$ is the coefficient of partial pressure, or total normal stress, borne by species i. They propose that in its simplest form this coefficient could take the form

$$\psi^{p,L} = \phi^L + b\phi^L\phi^S, \tag{2.14a}$$
$$\psi^{p,S} = \phi^S - b\phi^L\phi^S, \tag{2.14b}$$

where $i = L$ or S for large or small particles, respectively, and b is a positive unknown model parameter. Then, their model predicts

$$\phi^L(v^L - v) = -\frac{b\phi^L\phi^S}{c_D} g\cos\theta - \frac{d}{c_D}\frac{\partial \phi^i}{\partial y}, \tag{2.15a}$$
$$\phi^S(v^S - v) = \frac{b\phi^L\phi^S}{c_D} g\cos\theta - \frac{d}{c_D}\frac{\partial \phi^i}{\partial y} \tag{2.15b}$$

for the segregation flux of large and small particles, respectively. This form has a clear advantage in its elegantly simple predictive form for segregation fluxes. However, the expressions for the partition coefficients are untested. As discussed in the introduction,

other groups have suggested other forms for the partition coefficients, the drag law, and other details, though the essence is arguably similar to (2.13).

Since there is no distinction between contact and kinetic stresses in the Gray–Thornton–Chugunov model framework, compared to our (2.11), equation (2.13) is missing a term that scales with the kinetic stress gradient. Given that kinetic stresses are typically minimal in dense sheared systems, it is not at first clear that their gradients should be significant, particularly compared to the gravity term. We investigate this issue and related questions in the following sections.

Here, we make no initial assumptions or approximations for the forms of the stress partition coefficients and, rather, use simulations to investigate their dependence on mixture concentrations and the associated relative importance of the terms in (2.11). In the following sections, we test the plausibility of the theory presented in (2.11) and (2.12), in particular, the relative importance of the driving force associated with the kinetic stress gradient $\Phi^i_{\sigma k}$ (2.12*a*) using DEM simulations of granular mixtures. We also investigate the variability of the associated linear diffusion and drag coefficients, d and c_D, and the stress partition coefficients $\psi^{c,i}$ and $\psi^{k,i}$.

3. Discrete-element-method (DEM) simulations

We test our theory using DEM simulations, first introduced by Cundall & Strack (1979), of mixtures of different-sized spherical particles in a thin rotated drum. The boundary conditions and mixtures are similar to those described by Hill & Zhang (2008), where we demonstrated a good agreement between simulations and experimental measurements. We use a nonlinear soft sphere contact force model. As is common, the particle deformations resulting from particle–particle contacts are represented by small overlaps between particles and related to interparticle forces. The model we use follows Hertz–Mindlin contact theory with damping components related to the coefficient of restitution as developed by Tsuji, Tanaka & Ishida (1992) and Coulomb sliding friction:

$$F_n = -k_n\delta_n^{3/2} - \eta_n\delta_n^{1/4}\dot{\delta}_n, \tag{3.1}$$

$$F_t = \min\left\{-k_t\delta_n^{1/2}\delta_t - \eta_t\delta_n^{1/4}\dot{\delta}_t,\ \mu F_n\right\}, \tag{3.2}$$

where F_n and F_t are the contact forces in the directions normal and tangential to the contact plane between two contacting particles, δ_n and δ_t are the corresponding deformations, and μ is the coefficient of friction. The coefficients in the force model are related to material properties of the two contacting particles as presented in table 1. Since the two species differ only in mean size, and the behaviour of the flowing particles is relatively independent of particle property (e.g. Larcher & Jenkins 2009*a*) the choice of material properties is arbitrary. Here, we chose values similar to granite for the particles (e.g. Ide 1935; Simmons & Brace 1965). We specify these in table 2.

We perform the simulations using the boundary conditions of a circular drum with curved steel walls (properties specified in table 2). We use periodic boundaries in the axial direction (no front and back walls in figure 1(*a*) inset) to eliminate sidewall segregation effects (e.g. Hill & Zhang 2008). To calculate contact forces between the particles and the curved drum boundary, we follow the equations in table 1, using the approximation that the size and mass of the drum walls are infinite (compared to those of the particles). The drum diameter $D = 72$ mm; the thickness (periodic length in the axial direction) is $t = 30$ mm.

We partially 'fill' the drum with binary mixtures of particles of diameter $d = 2$ and 3 mm, with a 10 % variability in particle size of each constituent to

Variable	Formulae
k_n	$(4/3)\sqrt{R_{eff}}E_{eff}$
k_t	$8\sqrt{R_{eff}}G_{eff}$
η_n	$\alpha\sqrt{m_{eff}k_n}$
η_t	$\alpha\sqrt{m_{eff}k_t}$
R_{eff}	$(1/R_1 + 1/R_2)^{-1}$
E_{eff}	$[(1-\nu_1^2)/E_1 + (1-\nu_2^2)/E_2]^{-1}$
G_{eff}	$[2(1+\nu_1)(2-\nu_1)/E_1 + 2(1+\nu_2)(2-\nu_2)/E_2]^{-1}$
m_{eff}	$(1/m_1 + 1/m_2)^{-1}$

TABLE 1. Formulae for calculating stiffness and damping coefficients in (3.1) and (3.2). Subscripts 1 and 2 refer to each of the two particles in contact; $\alpha = 0.07$, corresponding to a typical restitution coefficient of 0.9; E_i, ν_i, m_i and R_i are the Young's modulus, Poisson's ratio, mass and radius respectively of particle i.

Material	Elastic modulus E (GPa)	Density ρ (kg m^{-3})	Poisson's ratio ν
Granite (particles)	29	2650	0.15
Steel (drum walls)	210	7850	0.3

TABLE 2. Material properties of particles and drum walls in DEM simulations. Coefficient of friction $\mu = 0.4$ for particle–particle interactions and 0.3 for particle–drum interactions.

minimize potential crystallization. To prepare each system, we release a random array of the binary mixture into the drum and rotate the drum at a speed of $\omega \approx 16$ rotations per minute (r.p.m.). The flow dynamics reach steady state relatively quickly (see figure 1*a*). At this speed the flowing layer is inclined at an angle of $\theta \approx 30^\circ$ (figure 1*a*) relative to the horizontal.

We study the segregation dynamics for five different concentrations of large particles (by volume) in the mixture: 10 %, 25 %, 50 %, 75 % and 90 %. We run three simulations for each mixture with different initial random configurations of particles. We calculate kinematics and stresses throughout each simulation as briefly described in §§ 3.1 and 3.2. We average over the results from the three simulations for each condition, over relatively short times in the segregation process (typically 0.5 s intervals), and over relatively small spatial bins (typically ≈10 mm wide × 0.2 mm high), as detailed below.

3.1. *Calculations of the kinematics*

To calculate the relevant kinematics for this study, we focus on the central 1/7 of the drum (as indicated in the inset to figure 1*a*) where the flow is relatively uniform in the x-direction. We divide this region into equal sized bins in the y-direction of width $\Delta y = 0.2$ mm. We calculate kinematic quantities by considering the contribution from the part of each particle j within a bin of width Δy centred at y (as described, for example, in Hill, Gioia & Tota 2003). For instance, $f^n(y) = \sum_\tau[\sum_j V^n_{\tau j}/NV_{bin}]$ and $v^n(y) = \sum_\tau[(\sum_j v^n_{\tau j}V^n_{\tau j})/(\sum_j NV^n_{\tau j})]$, where τ refers to the τth time step of which there are N, and j refers to the jth particle (of species n) that is partly or fully in this bin

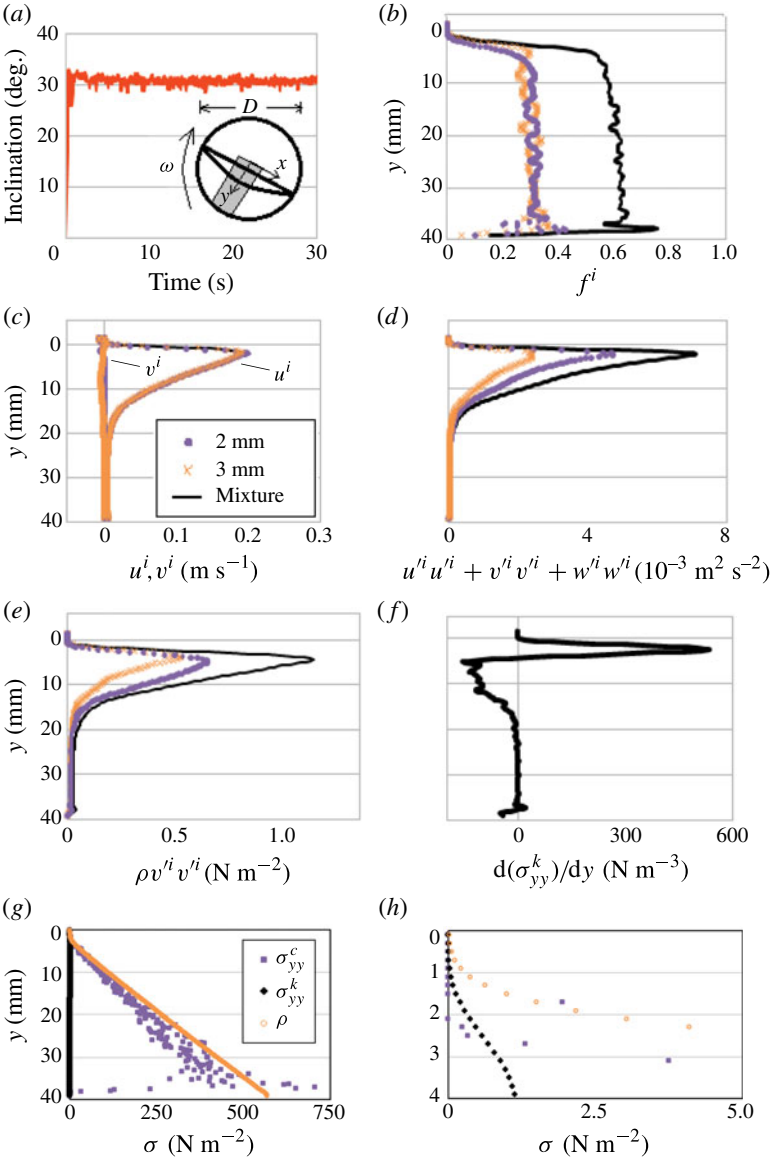

FIGURE 1. (Colour online) Some dynamics of a mixture with 50 % 3 mm (large) and 2 mm (small) particles rotated in a thin drum (details in § 3). (*a*) Evolution of the surface inclination, determined by locating the top particle in each of 15 vertical bins equally dividing the drum and applying a least-squares linear fit to their centroids. The inset indicates the region of the drum (the central 1/7) from which the data presented in (*b–g*) are calculated. (*b*) Solid fraction of each species and the mixture. (*c*) Velocity of each species and the mixture parallel and normal to the flow. (*d*) The velocity variance of each species and of the mixture. (*e*) The component of the kinetic stress in the direction normal to average flow for each species ($\rho^i v'^i v'^i$) and also for the mixture ($\sum_i (\rho^i v'^i v'^i)$). (*f*) Gradient of the kinetic stress of the mixture. (*g*) Contact and kinetic stresses of the mixture normal to flow, and lithostatic pressure (weight of overlying particles per unit area). (*h*) Close-up of (*g*) near the top of the flowing layer where the contact and kinetic stresses are of the same order of magnitude.

(at time step τ); $V_{\tau j}^{n}$ and $v_{\tau j}^{n}$ are the volume and velocity of that particle, respectively, and V_{bin} is the total volume of the bin ($V_{bin} = (D/7)\, t\, \Delta y$, except at the very bottom where the bins meet the curved drum wall).

3.2. *Calculations of the stresses*

To calculate the kinematic stress, we follow similar steps to those described for the kinematic variables described above. We calculate $\sigma_{yy}^{k,n}(y) = \rho^{n}\overline{v'^{n}v'^{n}}(y)$ (the y-component of the normal kinetic stress of species n) by considering the contribution from the part of each particle j within a bin of width Δy centred at y both to $\rho^{n} = \rho_{m} f^{n}$ and to $\overline{v'^{n}v'^{n}} = \overline{(v_{\tau j}^{n} - v(y))^{2}}$ (see Fan & Hill 2011*b* for details). As specified in § 2.2, $\sigma_{yy}^{k}(y) \equiv \sum_{n} \sigma_{yy}^{k,n}(y)$.

To calculate the local contact stress at each position y, we consider each interparticle contact K in a bin of width Δy centred at y (as in Fan & Hill 2011*b*). Then, we sum the stresses associated with each interparticle contact in each region, as in Kuhl *et al.* (2000) and Campbell (2002). The contribution from each contact K to the total contact stress tensor is:

$$\boldsymbol{F}_{ijK} \otimes \boldsymbol{l}_{ijK} \tag{3.3}$$

where $\boldsymbol{l}_{ij_K}$ is the vector from the centre of particle i to the centre of particle j. So for the mixture we have:

$$\boldsymbol{\sigma}^{c}(y) = \frac{\displaystyle\sum_{\tau=1}^{N} \sum_{K=1}^{N_c(y,\tau)} \boldsymbol{F}_{ij_K} \otimes \boldsymbol{l}_{ij_K}}{NV_{bin}}. \tag{3.4}$$

Here, $\boldsymbol{F}_{ij_K}$ is the force of particle i on particle j associated with the Kth contact, of which there are $N_c(y, \tau)$ in this bin (centred at time step τ. There are N such time steps.

For each constituent, the contribution of a particular contact between two particles of the same species to the partial stress of that constituent takes the same form as specified in (3.3). However the contribution of a contact between disparate particles to the partial stress tensor of each constituent scales with their relative size. Specifically, for a contact K between particle i of species n and particle j of species m, the contribution to the partial stress tensor of species n is:

$$\boldsymbol{F}_{ijK} \otimes \boldsymbol{r}_{ijK}, \tag{3.5}$$

where

$$\boldsymbol{r}_{ijK} = \frac{r_i}{r_i + r_j} \boldsymbol{l}_{ijK}. \tag{3.6}$$

We note that this definition is slightly different from that outlined in Fan & Hill (2011*b*), where the contact stress contribution was split equally between the two species regardless of relative size. Equations (3.5) and (3.6) are equivalent to those shown by Weinhart *et al.* (2012) to be the only mathematically consistent form for a different but highly related problem involving stresses shared by boundary particles and flowing particles. For each collision between disparate particles, this change in definition results in a higher portion of the collisional stress being attributed to the larger of the two particles in contact (and a smaller portion to the smaller particle), which has implications for the form of the partition coefficient as we discuss in § 5.

The total contact stress for constituent n in each bin is the sum of contributions from contacts between particles of the same species n and from contacts between

particles of the same species n and particles of disparate species m. In this bin centred at y:

$$\boldsymbol{\sigma}^{c,n}(y) = \frac{1}{NV_{bin}} \sum_{\tau=1}^{N} \left[\sum_{Kn=1}^{N_{cn}(y,\tau)} \boldsymbol{F}_{ij_{Kn}} \otimes \boldsymbol{l}_{ij_{Kn}} + \sum_{Km=1}^{N_{cm}(y,\tau)} \boldsymbol{F}_{ij_{Km}} \otimes \boldsymbol{r}_{ij_{Km}} \right]. \tag{3.7}$$

Here, at time step τ (of which there are N): $\boldsymbol{F}_{ij_{Kn}}$ is the force of particle i on particle j associated with the Knth contact (of which there are $N_{cn}(y, \tau)$) of two particles of the same species n; $\boldsymbol{F}_{ij_{Km}}$ is the force of particle i on particle j associated with the Kmth contact (of which there are $N_{cm}(y, \tau)$) of two particles of different species (n and m); $\boldsymbol{l}_{ij_{Kn}}$ is the vector from the centre of particle i to the centre of particle j, and $\boldsymbol{r}_{ij_{Km}}$ is the vector from the centre of particle i to the centre of particle j, scaled according to (3.6).

The calculation of contact stress in (3.7) is a relatively common method for representing the local contact stresses in a granular mixture (e.g. Alam & Luding 2003), though we note that it is not uncommon to apply an additional smoothing of each contact stress around the corresponding point of contact. Since the choice is somewhat arbitrary and here we are concerned with segregation trends, we do not apply any smoothing algorithm to our calculations of bulk contact stresses, which renders our fields somewhat noisy. We explore the effects of different smoothing algorithms on our data in a paper that is currently in preparation.

4. Drum simulation results

4.1. *Basic dynamics of dense sheared flow in a drum*

Figure 1 presents some basic features of the mixture dynamics of a segregating 50/50 mixture of particles in a drum when the particles are still well mixed (e.g. figure 1*b*). These results were obtained by averaging over a 500 ms period. (The analogous kinematics for all mixtures resembles, qualitatively, those shown in figure 1 for the 50/50 mixture.) Here and in the rest of the paper we present the kinematic properties calculated for the central 1/7 of the drum (as illustrated in the inset to figure 1*a*) where the flow is uniform in the streamwise direction. We chose (somewhat arbitrarily) $y = 0$ to represent the point at which the total solid fraction of the mixture reaches 0.1 %, coinciding, approximately, with the centre of the drum. As has been previously described (Bonamy, Daviaud & Laurent 2002; Jain, Ottino & Lueptow 2002; Hill *et al.* 2003; Gioia, Ott-Monsivais & Hill 2006), the very top of the flowing layer is quite sparse but within $y \approx 2$–3 particle diameters, the solid fraction of the mixture nearly reaches its maximum value. In the mixtures we investigate, (e.g. figure 1*b*), f reaches its maximum value of $\approx$0.6 at $y \approx 5$ mm. The streamwise average velocity (figure 1*c*) is maximum within the sparse region (in figure 1*c*, at $y \approx 2$ mm) and drops nearly to zero within $\approx$10 particle diameters ($y \approx 20$ mm for the data in figure 1*c*). Functional forms have been studied in more detail in previous publications (Bonamy *et al.* 2002; Jain *et al.* 2002; Hill *et al.* 2003; Gioia *et al.* 2006). The streamwise velocities are essentially the same for both components as in previous reports (Hill & Zhang 2008), but the normal velocities are not, more easily seen in the plots of the normal fluxes, which we present shortly. We identify the dense flowing layer as the region between where the density has essentially reached a plateau and where the velocity decreases to zero, 5 mm $\leqslant y \leqslant$ 20 mm. The sum of the velocity variances, a measure of the 'kinematic granular temperature' (e.g. Hill & Zhang 2008), peaks near the free surface (figure 1*d*); while the normal kinetic stress, σ^k_{yy} (figure 1*e*) peaks a bit lower, at the top of the dense region, coinciding with the near-plateau in the density

of the mixture ($\rho = \rho_m f$). It follows that $\mathrm{d}\sigma^k_{yy}/\mathrm{d}y$ (figure 1*f*) is negative throughout the dense region of the flowing layer; its peak is only slightly (∼0.1 mm) lower in the dense flowing layer.

We plot the stresses associated with (2.5), i.e. σ^c_{yy}, σ^k_{yy} and a lithostatic pressure $p(y) = \rho g y \cos\theta$, in figure 1(*g*,*h*). Throughout most of the depth, the weight is borne by σ^c_{yy}, and both σ^c_{yy} and p increase roughly linearly with depth. Only very near the top surface does σ^k_{yy} comprise a significant fraction of the total local stress. Based on these observations, it is tempting to discount the influence of the kinetic stress σ^k_{yy} on the segregating behaviour of the mixture. However, we note that the form of (2.11) suggests that the segregation term involving the kinetic stress scales with its gradient, $\mathrm{d}\sigma^k_{yy}/\mathrm{d}y$, and with the difference between the two partition coefficients, $(\psi^{c,i} - \psi^{k,i})$. While σ^k_{yy} may appear negligibly small, its gradient and the difference between $\psi^{c,i}$ and $\psi^{k,i}$ are not necessarily insignificant, and hence the contribution from kinetic stress effects should not be neglected automatically.

4.2. *Segregation behaviours*

Figure 2 shows the segregation kinematics of the 50/50 mixture near the beginning and end of segregation. For the first row (figure 2*a*–*c*), the data are averaged over the second 0.5 s of rotation, after the initial transients have dissipated. At this stage, the constituents are well-mixed (figure 2*a*,*b*), and the vertical flux $f^i \Delta v^i = f^i(v^i - v)$ is the greatest (figure 2*c*). In the dense region, the large particles have a negative flux and segregate upward toward the free surface. This relative segregation flux is greatest near the centre of the dense flowing layer. Snapshots of the particles in the centre of the dense flowing layer are shown in figure 2(*d*–*f*) as the segregation progresses. Vertical segregation in the flowing layer is frozen into a radial segregation pattern as illustrated in figure 2(*g*,*h*). Somewhat later in the simulation, a snapshot of the mixture (figure 2*i*) and the plot of the solid fractions of the components (figure 2*j*) show the constituents to be well-segregated. At this time, the flux (figure 2*k*) has dropped nearly to zero everywhere.

We plot the most striking details of these segregation dynamics for all mixtures in figure 3. Specifically, for each, we include a snapshot of the near steady-state segregation patterns in row (*a*), the corresponding plot of the solid fractions f^i in row (*b*), and the early-time segregation fluxes $f^i \Delta v^i$ in row (*c*). In all cases, the large particles segregate upward in the flowing layer and toward the outside of the drum. However, the details vary slightly from one to the next in terms of the flux magnitudes and relative concentrations of the two constituents as they vary with time.

To monitor the time dependence of the segregation, in figure 3(*d*) we plot a measure of the segregation, namely the standard deviation of mean concentration S of the large particles, as a function of time (t):

$$S(t) = \sqrt{\sum_{j=1}^{N_{bin}} (\phi^L_j(t) - \langle \phi^L \rangle)^2(t)/(N_{bin} - 1)}, \tag{4.1}$$

where $N_{bin} \approx 185$ is the number of bins in the y-direction, ϕ^L_j is the concentration of large particles in bin j, and $\langle \phi^L \rangle$ is the global concentration of large particles in the system (e.g. 0.5 in the 50/50 mixture). In all cases, S vs. t is fitted well by the function:

$$S^*(t) = S_f - S_o \exp\left(-\frac{t - t_d}{\tau_c}\right), \quad t > t_d, \tag{4.2}$$

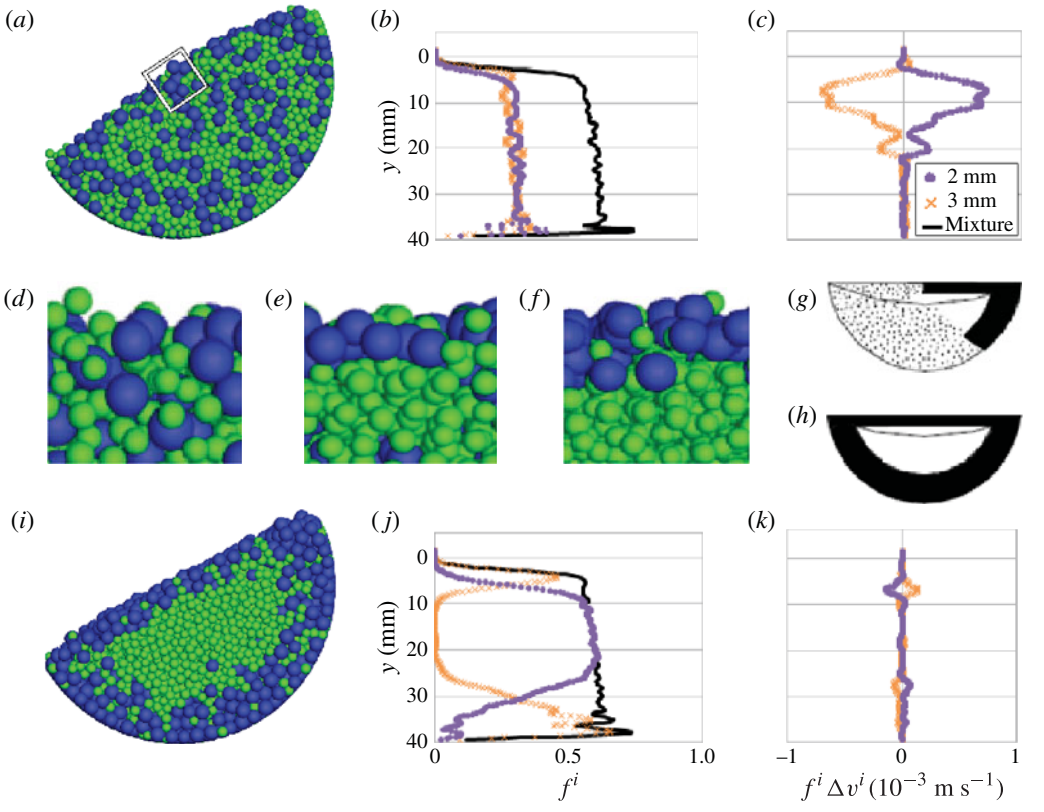

FIGURE 2. (Colour online) (*a–c*) Details of a 50/50 mixture in a drum near the beginning of the simulation ($t = 0.5$–1 s) when the constituents are well-mixed: (*a*) a snapshot; (*b*) solid fraction f^i profile of each constituent i and the mixture; (*c*) vertical flux profile $f^i \Delta v^i = f^i(v^i - v)$ of each constituent. (*d–f*) Snapshots from the central part of the flowing layer in the simulations, denoted by the dashed box in (*a*): (*d*) initial state; (*e*) 5 s into the simulation; (*f*) the steady segregated state of the system. (*g*,*h*) Sketches illustrating how the segregation in the top flowing layer is recorded into a radial segregation pattern in the solid-like granular materials in the majority of the drum (from Hill, Gioia & Amaravadi 2004). (*i–k*) Details from the same simulation, after ≈30 s of rotation ($t = 29.5$–30 s), when segregation has essentially reached steady state. Corresponding to (*a–c*), (*i*) shows a snapshot, (*j*) solid fraction profile of each constituent and the mixture, and (*k*) vertical flux profile of each constituent. As in figure 1, the plotted data are calculated from the middle 1/7 of the drum (as illustrated in the inset of figure 1*a*), and obtained by averaging over a 500 ms period.

where S_f represents the value of S at steady state; $S_f - S_o$ is the average initial segregation value (calculated by averaging the data from $t = 0.5$ to 1.0 s); t_d represents a 'delay time', that is, an initial (transient) time before the segregation is apparent in the concentration variations in the centre of the drum (∼1–2 s), and τ_c represents the time constant associated with the rate of segregation. The fitting coefficients (S_f, S_o, t_d and τ_c) associated with each concentration are shown in table 3. In all cases, segregation is well-underway by $\tau_c \approx 5$–6 s, and nearly finished by $3\tau_c \approx 15$–18 s, so we terminate our simulations at $t = 30$ s.

https://doi.org/10.1017/jfm.2014.271 Published online by Cambridge University Press

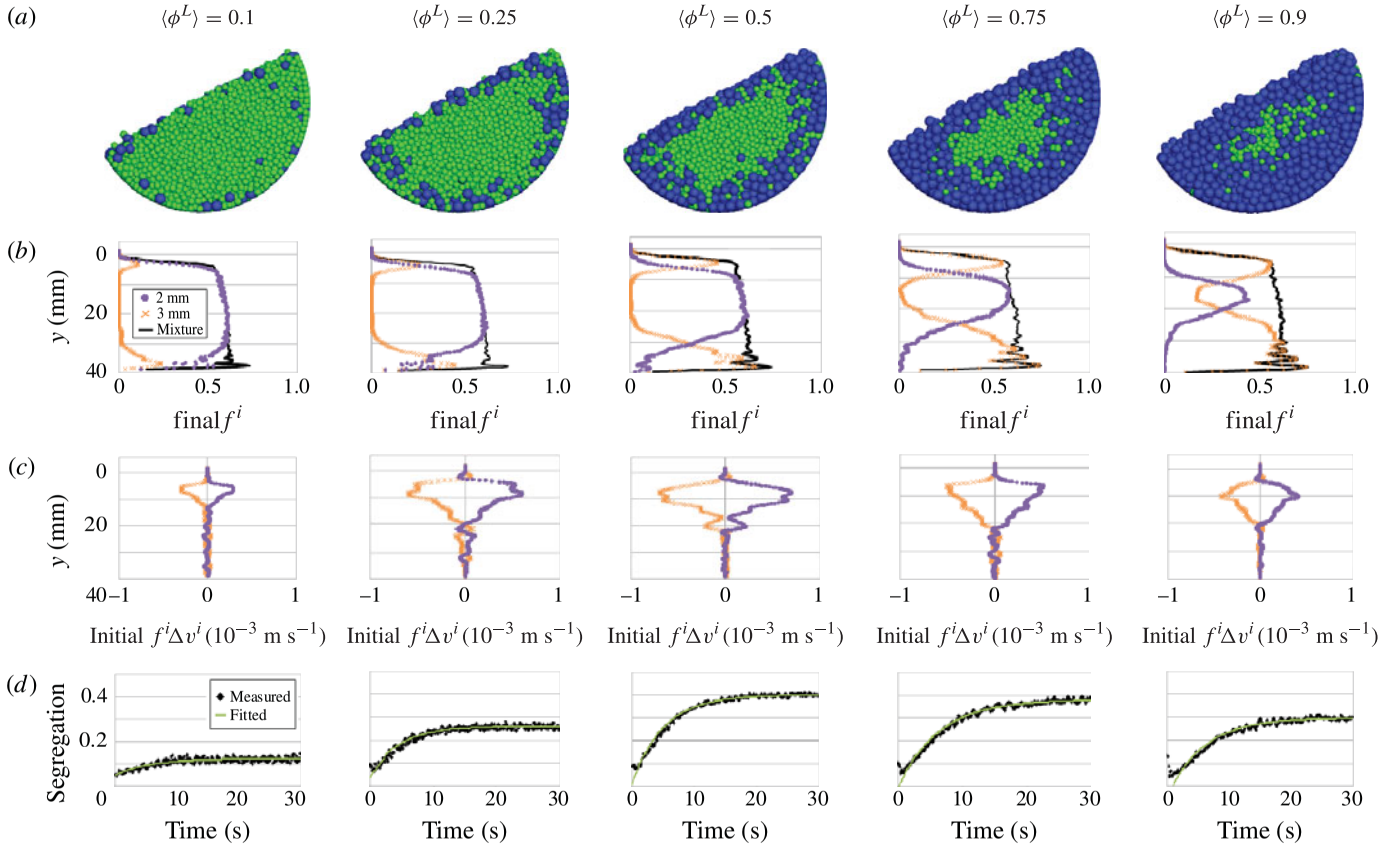

FIGURE 3. (Colour online) Segregation of mixtures with different concentrations of 3 mm (large) particles, $\langle\phi^L\rangle$, increasing left to right from 0.1 to 0.9. (*a*) Snapshots of segregated mixtures. (*b*) Solid fraction of each species and mixture corresponding to snapshots above, after ≈30 s of rotation. (*c*) Flux ≈0.5 s after beginning rotation. Plots (*b*) and (*c*) were obtained by averaging over a 500 ms period. (*d*) Evolution of segregation over time. The measured segregation $S(t)$ is calculated using (4.1), and the fitted expression $S^*(t)$ is given in (4.2).

	$\langle\phi^L\rangle$				
	0.10	0.25	0.50	0.75	0.90
S_f	0.12	0.26	0.40	0.38	0.29
S_o	0.06	0.18	0.32	0.31	0.25
t_d (s)	1.05	1.05	1.05	1.63	1.89
τ_c (s)	5.00	4.55	5.00	6.25	5.56

TABLE 3. Values of fitting coefficients for $S^*(t) = S_f - S_o \exp(-(t - t_d/\tau_c))$ for the data associated with each mixture (plotted in figure 3*d*).

5. Evolution of stress partition during segregation

To evaluate the magnitude of the shear-driven and gravity-driven segregation 'driving forces' in (2.11) (i.e. $\Phi^i_{\sigma k}$ and Φ^i_g, in (2.12*a*,*b*)), we investigate the evolution of the stresses and the stress partition coefficients in the 50/50 mixtures as segregation evolves. We focus our discussion primarily on the mixture with 50 % by volume each of small and large particles, as the qualitative details are similar for all mixtures. In figure 4 we plot profiles of the concentrations of the constituents $\phi^i(y)$, profiles of the contact stresses $\sigma^{c,i}(y)$ associated with each constituent and the mixture, and profiles of the kinetic stresses $\sigma^{k,i}(y)$ associated with each constituent and the mixture near the beginning of the simulation and at $t = \tau_c$, $2\tau_c$ and $3\tau_c$. At early times, $t = 0.5$–1 s, when the system is well-mixed (figure 4 top row), $\sigma^{c,i}(y)$ for both constituents increases essentially linearly with depth, and in fact, $\sigma^c(y)$ is shared equally at every depth y ($\sigma^{c,L}(y) \approx \sigma^{c,S}(y)$). In contrast, at these early times, $\sigma^{k,i}(y)$ is not the same for the two constituents, and visual inspection indicates that at every depth, $\sigma^{k,S}(y) \geqslant \sigma^{k,L}(y)$. As the segregation evolves, the results for $t = \tau_c$, $2\tau_c$ and $3\tau_c$ indicate that the degree to which each constituent bears the kinetic and contact stresses evolves with the concentration, as it should: the higher the concentration of one constituent, the larger the percentage of the total stress it bears. For example, at depths where there are very few large particles (e.g. at $t = 3\tau_c$ from $y \approx 10$ to 20 mm where $\phi^L(y) \approx 0$ and $\phi^S(y) \approx 1$), $\sigma^{k,S}(y) \approx \sigma^k(y)$ and $\sigma^{c,S}(y) \approx \sigma^c(y)$, as one might trivially expect. For intermediate values of $\phi^S(y)$ and $\phi^L(y)$ (that is, not close to 0, 0.5, or 1), the relative partitioning of the stresses is not so obvious from these stress plots alone.

To better visualize the spatially resolved partitioning of the contact and kinetic stresses between the constituents relative to their concentrations ϕ^i, we introduce two new variables, $R^{c,i} = \psi^{c,i}/\phi^i$ and $R^{k,i} = \psi^{k,i}/\phi^i$, as relative stress partition coefficients. In figure 5(*a*), we have plotted profiles of $R^{c,i}$ at each of the four time steps investigated in figure 4. At early times ($t = 0.5$–1 s and $t = \tau_c$), $R^{c,L} \approx R^{c,S} \approx 1$. At later times ($t = 2\tau_c$, $3\tau_c$) there is much more scatter particularly for $R^{c,L} = \psi^{c,L}/\phi^L$ where, for most of the depth, $\psi^{c,L} \approx \phi^L \approx 0$ so that a very small fluctuation in ϕ^L leads to a relatively large fluctuation in $R^{c,L}$.

To better reveal the trend throughout the segregation process, in figure 5(*b*), we include parametric plots of $\psi^{c,i}$ as a function of ϕ^i for the entire flowing layer except the very topmost sparse part (2 mm $\leqslant y \leqslant$ 20 mm). These plots are somewhat noisier for the earlier times for all but $\phi^i \approx 0.5$, probably because the sample size of points within the dense flowing layer where $\phi^i \neq 0.5$ is small. Otherwise, these plots indicate that for all times

$$\psi^{c,i} \approx \phi^i. \tag{5.1}$$

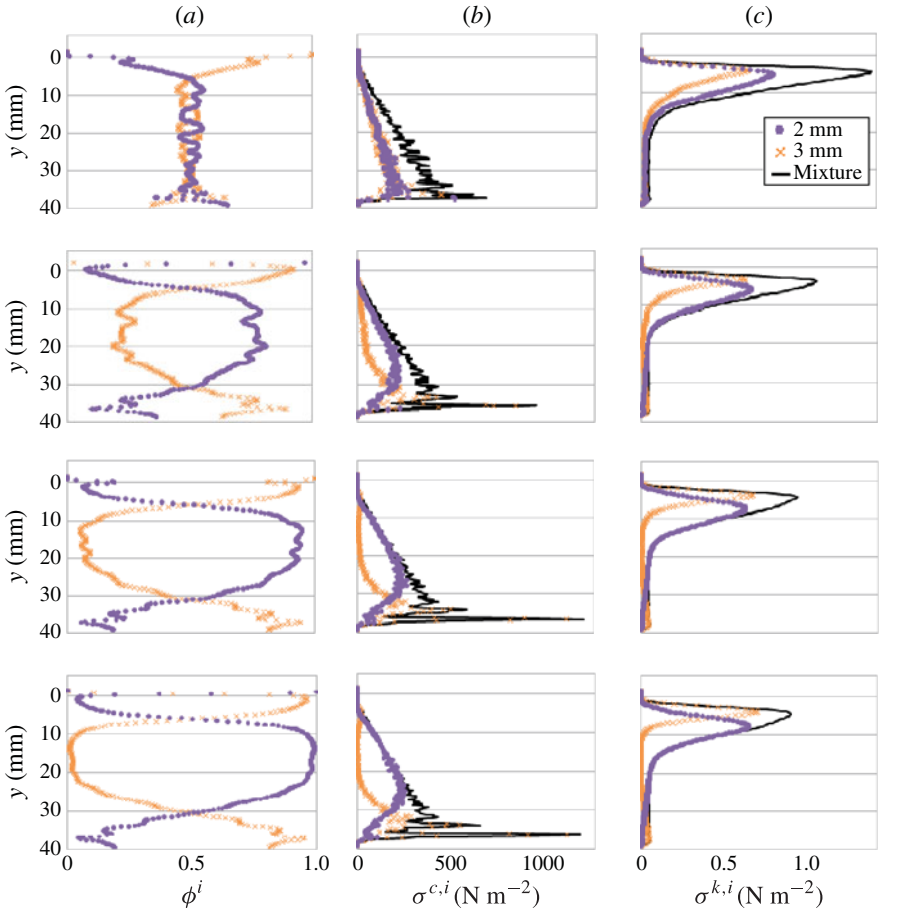

FIGURE 4. (Colour online) Concentration, contact and kinetic stresses corresponding to the 2 mm (small) and 3 mm (large) particles, and the mixture (50 % large particles), at different stages of segregation (top row: beginning segregation, $t = 0.5$–1 s; successive rows at increasing multiples of the time constant: τ_c, $2\tau_c$, $3\tau_c$). (*a*) Concentration of each species. (*b*,*c*) Contact and kinetic stresses normal to flow, of each species and the mixture. Apart from the first row, the plots were obtained by averaging over a 1 s period.

We note that this is somewhat different from what we reported in Fan & Hill (2011*b*) for vertical chute flow, where we found that $\psi^{c,L} < \phi^L$, and $\psi^{c,S} > \phi^S$. The difference appears primarily associated with the different form of (3.5), though when we used the improved form for the chute flow, we still found $\psi^{c,L} - \phi^L$ to be slightly negative and $\psi^{c,S} - \phi^S$ to be slightly positive. We are currently investigating whether this difference is associated with the uncertainty of the system, or if the stress partitioning is indeed different in the disparate systems.

Figure 5(*c*,*d*) shows that the dependence of $\psi^{k,i}$ on ϕ^i is somewhat more complicated. At all depths within the flowing layer except the very sparse top ($2\text{ mm} \leqslant y \leqslant 20\text{ mm}$) $R^{k,L} \leqslant 1$ and $R^{k,S} \geqslant 1$. In other words, the kinetic stress is not partitioned exactly according to constituent concentration in the mixture. Rather, except where $\phi^L = 1$ or 0, the small particles carry a disproportionate share of the kinetic stress; $\psi^{k,L} < \phi^L$ and $\psi^{k,S} > \phi^S$.

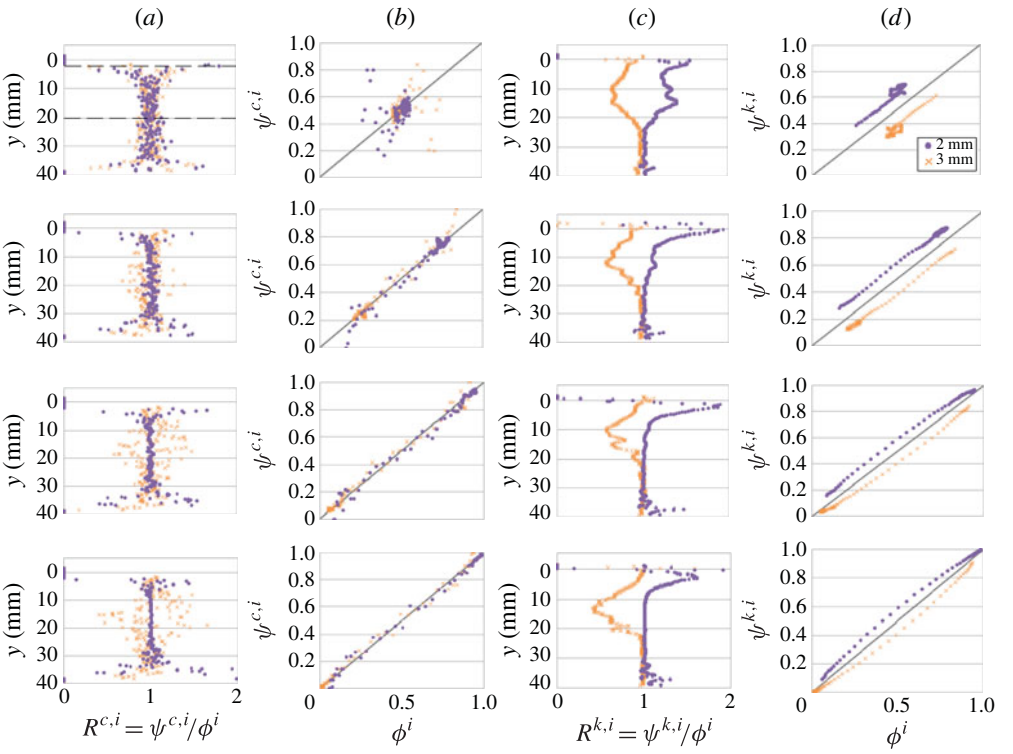

FIGURE 5. (Colour online) Ratios of $\psi^{c,i}$ to ϕ^i, and $\psi^{k,i}$ to ϕ^i at different stages of segregation for the mixture with 50 % large particles (top row: beginning segregation, $t = 0.5$–1 s; successive rows at increasing multiples of the time constant: τ_c, $2\tau_c$, $3\tau_c$). (*a*,*c*) Depth profile of the relative contact and kinetic stress partition coefficients of each species. Dashed line in the top graph of (*a*) demarcates the entire flowing layer except the very top sparsest part (2 mm $\leqslant y \leqslant$ 20 mm). (*b*,*d*) Contact and kinetic stresses (in the flowing layer only) of each species as functions of corresponding local species concentration. Apart from the first row, the plots were obtained by averaging over a 1 s period.

When we plot all data from figure 5(*d*) of $\psi^{k,i}$ as a function of ϕ^i, along with the set from the final half-second of the simulation for the 50/50 mixture (figure 6*a*), we find that the trend is similar throughout the simulation. We fitted a quadratic function to $\psi^{k,i}$ vs. ϕ^i for the data from $t = 29.5$ to 30 s and obtained the following empirical relationship:

$$\psi^{k,L}(\phi^L) \approx 0.39\left(\phi^L\right)^2 + 0.61\phi^L \tag{5.2a}$$

and subsequently,

$$\psi^{k,S}(\phi^S) = 1 - \psi^{k,L}(1 - (\phi^S)) \approx -0.39\left(\phi^S\right)^2 + 1.39\phi^S. \tag{5.2b}$$

Plotted with the data in figure 6(*a*), this appears to represent the data fairly well at all times for the 50/50 mixture. Further, when we plot this with the analogous data for the other mixtures at late times ($t = 29.5$–30 s) in figure 6(*b*), we see that the empirical fit represented by (5.2) represents the data well for all mixtures we simulated.

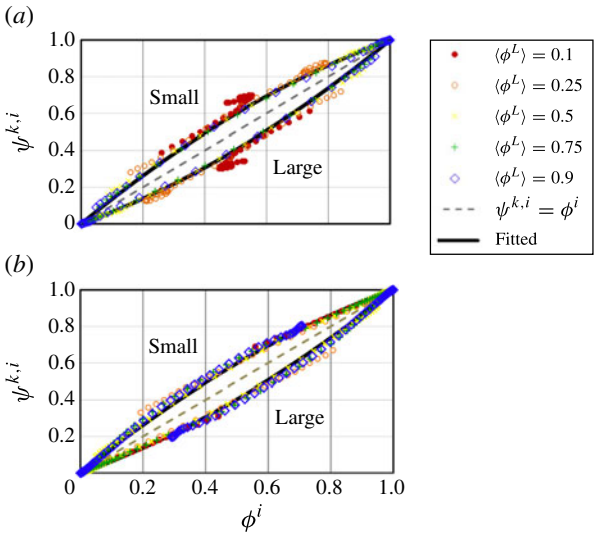

FIGURE 6. (Colour online) Kinetic stress ratio $\psi^{k,i}$ as a function of local concentration ϕ^i, in the flowing layer (see dashed line in figure 5*a*): (*a*) mixture with 50 % large particles, at different times during segregation; (*b*) mixtures of different global concentration, at the end of each simulation ($t \approx 29.5$–30 s). The fitted line in both (*a*) and (*b*) was obtained from the mixture with 50 % large particles, at the end of the simulation.

We note that this is similar to the form of the pressure coefficient suggested by Gray and colleagues (2.14). Here, we could write

$$\psi^{c,L} \approx \phi^L + b^c \phi^L \phi^S, \tag{5.3a}$$

$$\psi^{k,L} \approx \phi^L + b^k \phi^L \phi^S, \tag{5.3b}$$

with analogous equations (with minus signs) for the small particles. We find for our mixture that $b^c = 0$ and $b^k = -0.39$. Both our values for b are less than or equal to 0, unlike the positive value for the analogous total pressure partition coefficient suggested by Gray and colleagues.

Interestingly, these results with our associated segregation model indicate that the small particles, not the large particles, carry more of the stress in general, in particular, the kinetic stress. The result that $b^c = 0$ implies that gravity does not play a direct role in segregation, only implicitly through setting up the shear flow and associated kinetic stress gradient.

There is no quantitative explanation for these particular relationships; however the form of the kinetic stress partition coefficients is consistent with earlier results by Hill & Zhang (2008) indicating that smaller particles have higher velocity variances than larger particles in a mixture. Our preliminary calculations indicate that the predictions from the model for fluctuations from Hill & Zhang (2008) do not deviate significantly from the empirical fit of (5.2). The details do not affect the model and simulations described here, so we leave a detailed discussion to a future paper and focus the rest of this paper on comparing our segregation model to our simulation results.

We now incorporate our findings for the partial stress partition coefficients into the model summarized by (2.11). Specifically, since we found empirical forms of

$\psi^{c,i}(\phi^i)$ ($\approx\phi^i$) and $\psi^{k,i}(\phi^i)$ (given by (5.2*a*,*b*)), (2.11) predicts that

$$\Phi_T^i \approx \Phi_{T,\sigma kd}^i \equiv \Phi_{\sigma k}^i + \Phi_d^i = \left(\frac{\phi^i - \psi^{k,i}(\phi^i)}{\rho c_D}\frac{\partial \sigma_{yy}^k}{\partial y}\right) - \left(\frac{d}{c_D}\frac{\partial \phi^i}{\partial y}\right). \tag{5.4}$$

In this equation, we introduce the term $\Phi_{T,\sigma kd}^i$ to emphasize that after incorporating the empirical stress partition coefficients, the total theoretical flux is now made up of two components: (i) segregation along a kinetic stress gradient $\partial\sigma_{yy}^k/\partial y$ and (ii) the diffusion term. To obtain an estimate for c_D, we return to results from our simulation data at early times, and, for d, we use late-time results.

6. Model predictions compared with simulation results

In this section, we use the predictions from the model (5.4) in conjunction with simulation results with two goals in mind: (i) to determine functional forms for the model parameters c_D and d (coefficients of drag and diffusion), and (ii) to evaluate the effectiveness of the model in capturing the segregation fluxes at all times. Since we do not have physics-based predictive forms for the model parameters at this time, we evaluate the parameters c_D and d each at one specific time in the segregation process. We use results from early times to estimate the drag coefficient c_D and the results from later times to estimate the diffusion coefficient d. We then use these to determine the effectiveness of the model at all times in the simulation.

6.1. *Early time simulation results and drag coefficient estimate*

Near the beginning of each simulation when $t \approx 0.5$–1.0 s, the constituents are still relatively well-mixed and the mixture is uniform: $\partial\phi^i/\partial y \approx 0$. Based on this, at early times the segregation flux may be estimated by:

$$\Phi_T^i \approx \Phi_{T,\sigma k}^i = \frac{\phi^i - \psi^{k,i}(\phi^i)}{\rho c_D}\frac{\partial \sigma_{yy}^k}{\partial y}. \tag{6.1}$$

We use this to empirically determine c_D separately for each of our mixtures. To do this, for each mixture, we calculate the average simulated segregation flux profile $\Phi_M^i(y) = \phi^i(y)(v^i(y) - v(y))$ for $t \approx 0.5$–1.0 s (figure 7*b*). Then, we use the simulated concentration (figure 7*a*) and kinetic stress gradient profiles (e.g. figure 1*f*) with (5.2) and (6.1) to calculate $\Phi_{T,\sigma k}^i(y)\, c_D = (\phi^i - \psi^{k,i}(\phi^i))\,\partial\sigma_{yy}^k(y)/\partial y$. We then use these calculations with the method of least-squares fitting to find the value of $c_D(\phi^L)$ that minimizes the sum of the squares of the differences between $\Phi_{T,\sigma k}^i(y)\, c_D = (\phi^i - \psi^{k,i}(\phi^i))\,\partial\sigma_{yy}^k(y)/\partial y$ and $\Phi_M^i(y)\, c_D$ for each mixture of global concentration $\langle\phi^L\rangle$. We note that at these early stages, throughout the depth of the flowing layer, $\phi^L(y) \approx \langle\phi^L\rangle$. Thus we make the approximation that for each mixture, a single value of c_D (corresponding to $\phi^L = \langle\phi^L\rangle$) is sufficient.

Though only a single value of c_D is used for each mixture, the spatial dependence of $\Phi_T^i(y) = [(\phi^i - \psi^{k,i}(\phi^i))/\rho c_D]\partial\sigma_{yy}^k/\partial y$ on c_D obtained in this way is similar to the spatial dependence of $\Phi_M^i(y)$. Here, $\Phi_M^i(y)$ and $\Phi_T^i(y)$ obtained in this way may be compared for each concentration in figure 7(*b*). The best fit values for $c_D(\phi^L)$ are given in table 4 and plotted as a function of $\langle\phi^L\rangle$ in figure 8. There is no systematic variation of c_D with concentration, and the variability is relatively small. Thus, for the purposes of the calculations we present in the rest of this paper, we approximate c_D for all mixtures with a single value, the average of the results from these empirical fits: 6.3 s^{-1}.

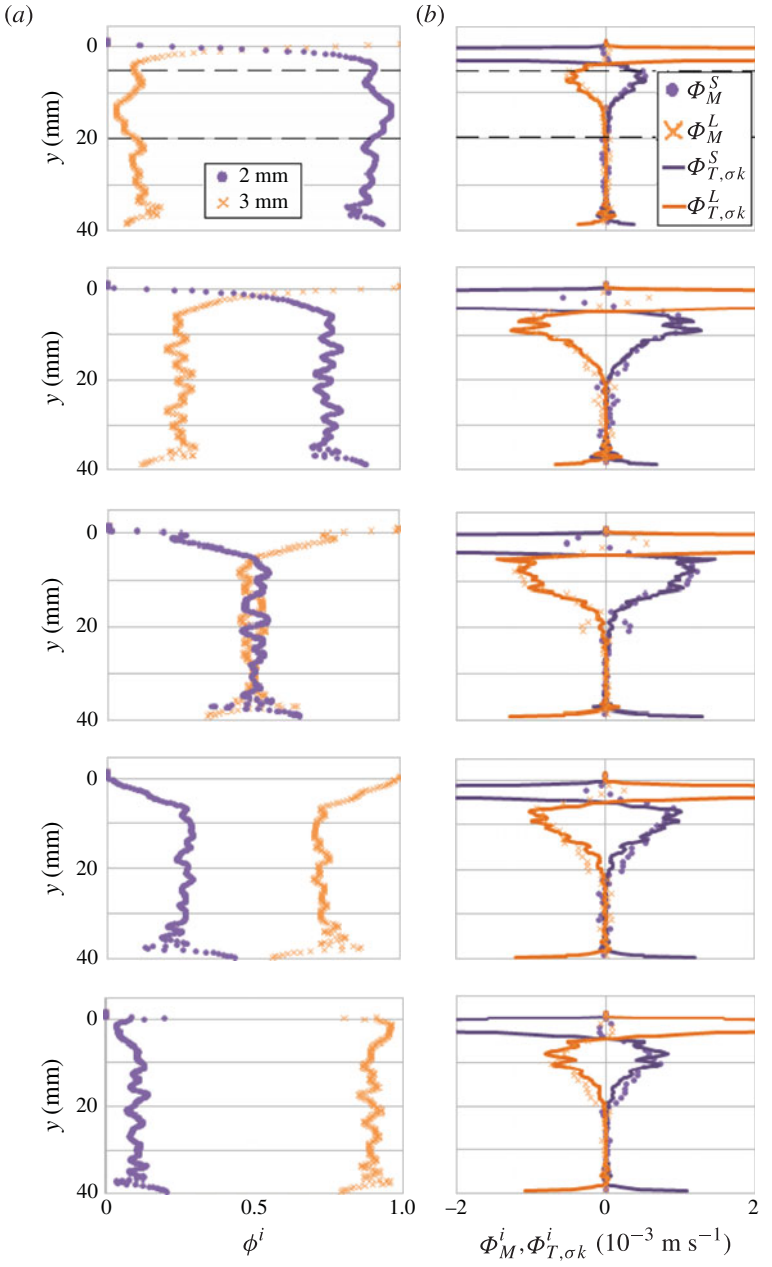

FIGURE 7. (Colour online) Concentrations and segregation fluxes from the simulations $\Phi_M^i = \phi^i \Delta v^i$ and segregation fluxes predicted from the model $\Phi_{T,\sigma k}^i = ((\psi^{c,i} - \psi^{k,i})/\rho c_D)\partial\sigma_{yy}^k/\partial y$. All data shown are from the initial stages of the simulations ($t =$ 0.5–1 s) for mixtures with different concentrations. Global concentration of large particles increases from top to bottom: $\langle\phi^L\rangle = 0.1, 0.25, 0.5, 0.75, 0.9$. (*a*) Local concentration of each species. (*b*) Measured and theoretical fluxes of each species. The drag coefficient c_D is determined with these data, based on least-squares fitting of $c_D\phi^i\Delta v^i$ to $((\psi^{c,i} - \psi^{k,i})/\rho)\partial\sigma_{yy}^k/\partial y$ in the dense portion of the flowing layer (typically, $y = 5$–20 mm, as denoted with dashed lines in the top graphs). The drag coefficients that best fit the data are given in table 4 and figure 8.

	$\langle\phi^L\rangle$					
	0.10	0.25	0.50	0.75	0.90	—
c_D (s^{-1})	6.6	5.3	6.8	7.4	5.3	6.3
d (m^2 s^{-2})	1.32×10^{-5}	8.93×10^{-6}	1.11×10^{-5}	9.66×10^{-6}	2.01×10^{-5}	1.26×10^{-5}

TABLE 4. Values of the drag coefficient c_D and diffusion parameter d, empirically determined for mixtures with different global concentrations of large particles as detailed in the text. The last column, the average values of c_D and d, are used for later comparisons.

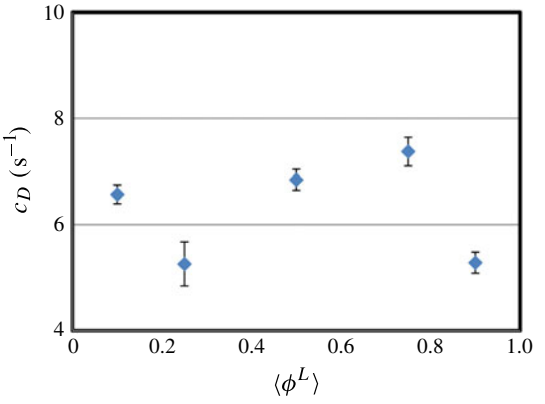

FIGURE 8. (Colour online) Drag coefficient c_D found from least-squares fitting of the model flux data to the simulated flux data is plotted as a function of global concentration of large particles $\langle\phi^L\rangle$. The error bars are derived from the sum of the least squares of the difference between each value of $c_D\phi^i\Delta v^i$ and $((\psi^{c,i} - \psi^{k,i})/\rho)\partial\sigma^k_{yy}/\partial y$ in the dense part of the flow indicated in figure 7, assuming these differences exhibit homoscedascity. They represent an uncertainty in c_D associated with a point-by-point difference between the theoretical and simulated values of the segregation fluxes.

6.2. *Late time simulation results and d estimate*

Near the end of the simulation, when $t \approx 29.5$–30.0 s (for each mixture), the simulated segregation flux $\Phi^i_M(y) = \phi^i(y)(v^i(y) - v(y)) \approx 0$. In other words, (5.4) predicts that at these later times,

$$\Phi^i_{\sigma k} = -\Phi^i_d. \tag{6.2}$$

That is,

$$\frac{\phi^i - \psi^{k,i}(\phi^i)}{\rho}\frac{\partial\sigma^k_{yy}}{\partial y} = d\frac{\partial\phi^i}{\partial y}. \tag{6.3}$$

To estimate d, we use the simulated data from each mixture averaged from $t \approx 29.5$ to 30.0 s, to calculate $\phi^i(y)$ for each mixture (figure 9, row 1) and $\sigma^k_{yy}(y)$ (e.g. similar to figure 4(*c*), row 3). From this, we calculate $\Phi^i_{\sigma k}(y)$ and $\Phi^i_d(y)/d$ for each mixture. We use these calculations with the method of least-squares fitting to find the value of d that minimizes the sum of the squares of the differences between the left- and right-hand sides of (6.3) (see figure 9) for each mixture in the dense portion of the flowing layer ($5\text{ mm} \leqslant y \leqslant 20\text{ mm}$).

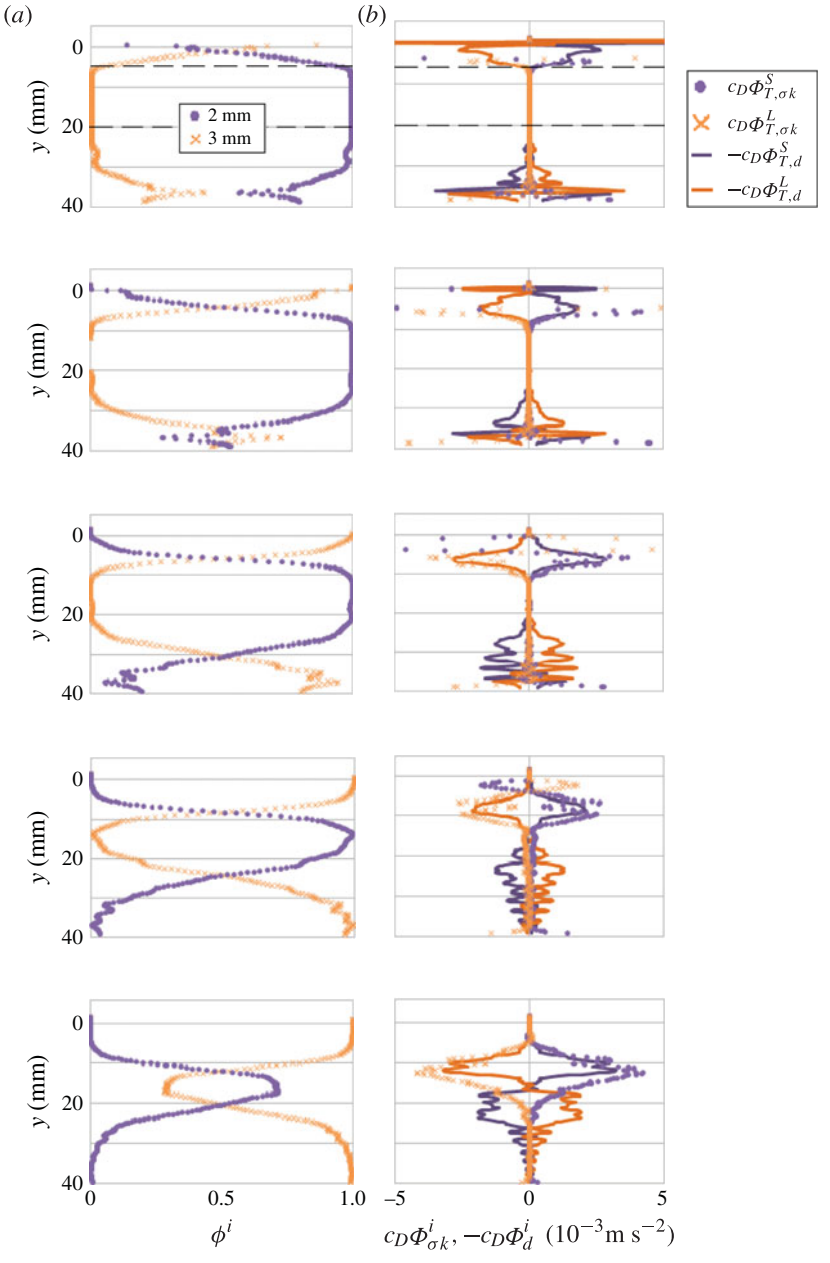

FIGURE 9. (Colour online) (*a*) Near-steady-state concentrations ϕ^i and (*b*) a comparison between the computational and theoretical segregation flux (multiplied by c_D). The data plotted in (*b*) were calculated according to $c_D\Phi^i_{\sigma k} = ((\psi^{c,i} - \psi^{k,i})/\rho)\partial\sigma^k_{yy}/\partial y$, and $c_D\Phi^i_d = d\partial\phi^i/\partial y$). Global concentration of large particles increases from top to bottom: $\langle\phi^L\rangle = 0.1, 0.25, 0.5, 0.75, 0.9$. The data were obtained by averaging over a 500 ms period near the end of the segregation process. The diffusion parameter d was determined by a least-squares fitting to minimize the difference between the computational and theoretical segregation flux in the dense portion of the flowing layer (5–20 mm, demarcated with dashed lines) in the first row. The values found for d in each case are given in table 4 and figure 10.

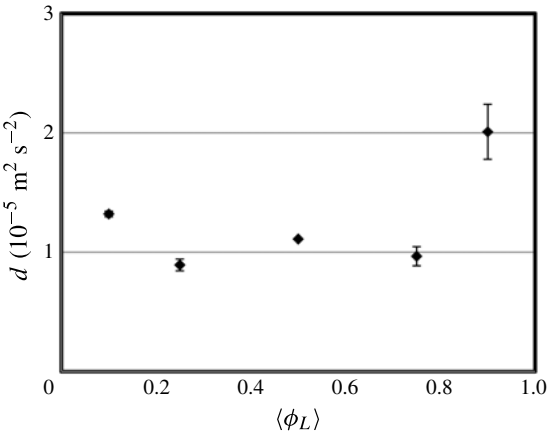

FIGURE 10. Diffusion parameter d, found from least-squares fitting of the left- and right-hand side terms of (6.3), is plotted as a function of global concentration of large particles $\langle\phi^L\rangle$. The error bars are derived from the sum of the least-squares of the difference between each value of $c_D\Phi^i_{\sigma k} = ((\psi^{c,i} - \psi^{k,i})/\rho)\partial\sigma^k_{yy}/\partial y$, and $c_D\Phi^i_d = d\partial\phi^i/\partial y$ in the dense part of the flow indicated in figure 9, assuming these differences exhibit homoscedascity. They represent an uncertainty in d associated with a point-by-point difference between the theoretical and simulated values of the segregation fluxes.

The results from this least-squares fitting may be seen in figure 9(*b*). While not as satisfying as those from fitting c_D shown in figure 7, the results within the dense flowing layer are not unreasonable, and the worst breakdowns occur where one would expect the behaviour to be different at the very top, where the flow is quite sparse ($y < 2$ mm) and in the creeping region ($y > 20$ mm).

The values of d from each mixture are included in table 4, and plotted in figure 10. Similar to our empirical results for c_D, there appears to be no systematic variation of d with concentration, and, in fact, the variation with $\langle\phi^L\rangle$ is rather small. Therefore, for purposes of the comparisons between simulation and theory in the rest of this paper, we use the average value of d, 1.26×10^{-5} m^2 s^{-2}.

6.3. *Theoretical predictions and simulation results for the flowing layer: evaluation during progression of segregation*

We now use the average values of c_D and d with (5.2) in (5.4) to predict the segregation flux profiles $\Phi^i_{T,\sigma kd}(y)$ at different times for all of our mixtures. We plot these with the simulated flux profiles $\Phi^i_M(y) = \phi^i(y)(v^i(y) - v(y))$ in figure 11.

In nearly all cases, the agreement between theoretical flux (with empirically determined coefficients) and measured fluxes from the simulations are remarkable. Notable deviations occur for high concentrations of large particles and later times, particularly near the top of the flowing layer. We hypothesize that this may be due to our approximation that the coefficients of drag and diffusion are independent of concentration and other dynamic variables. The diffusion coefficient d in particular appeared to vary significantly for the mixture with the highest concentration of large particles $\langle\phi^L\rangle = 0.90$. Indeed, for most of the mixtures, the evaluation of d took place in a region of the flowing layer where the concentration of small particles was quite high and the concentration of large particles quite low, so there may be significant

https://doi.org/10.1017/jfm.2014.271 Published online by Cambridge University Press

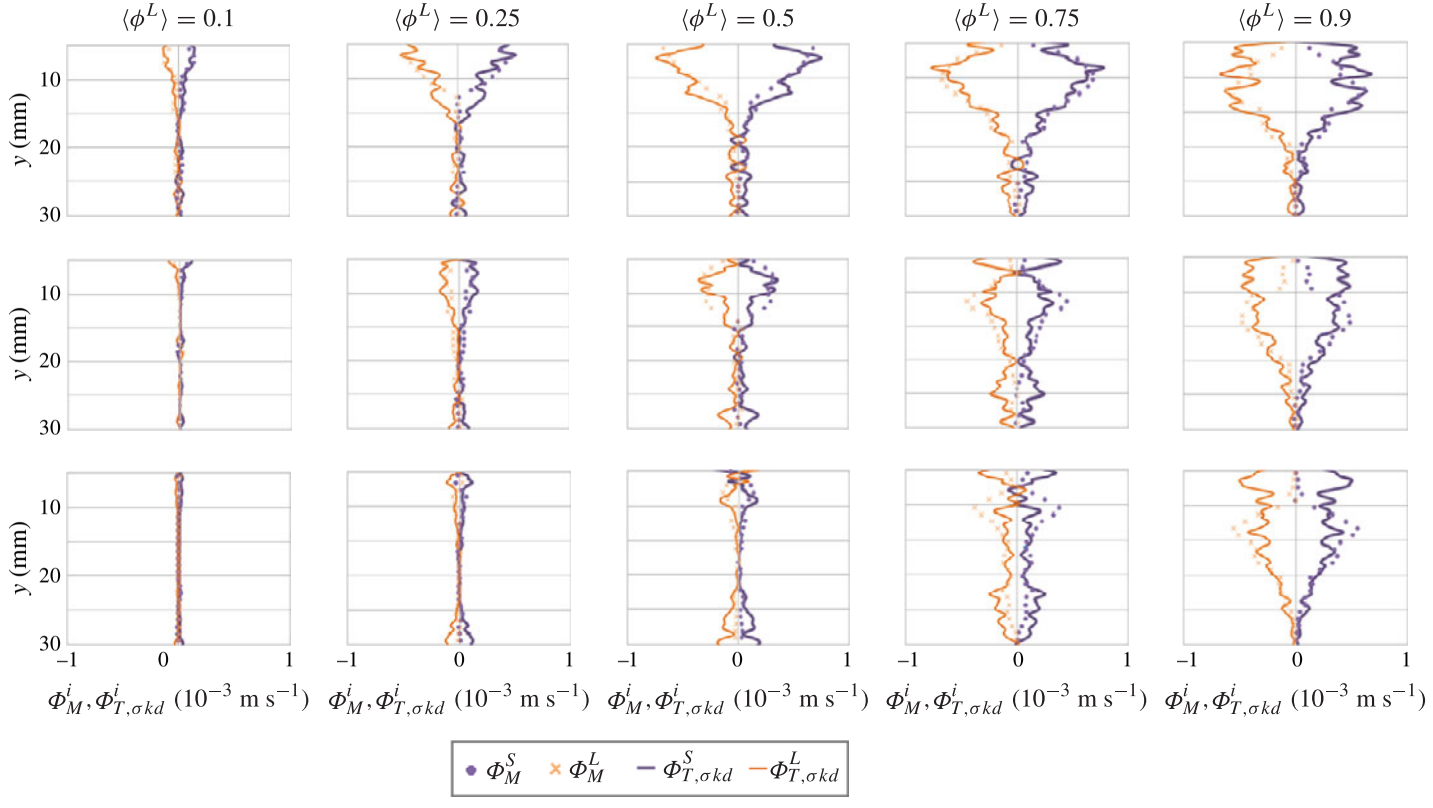

FIGURE 11. (Colour online) Simulated fluxes $\Phi^i_M = \phi^i \Delta v^i$ and theoretical fluxes $\Phi^i_{T,\sigma kd} = ((\psi^{c,i} - \psi^{k,i})/\rho c_D)\partial\sigma^k_{yy}/\partial y - (d/c_D)\partial\phi^i/\partial y$ at different stages of segregation for mixtures with different concentrations. Global concentration of large particles increases from 0.1 to 0.9 (from left to right), and time increases down the rows: $t = \tau_c, 2\tau_c, 3\tau_c$. These plots were obtained by averaging over a 1 s period.

variability of the diffusion coefficient with concentration that we were not able to capture with our evaluation. We are currently investigating a more rigorous evaluation of these coefficients that accounts for dependence on local mixture concentration.

6.4. *Comparison with related results*

It is informative to compare our model coefficients to those obtained in similar work. Marks *et al.* (2012) reported stress partition coefficients $\psi^{c,i}/\phi^i$ that scale with particle size ratio in the mixture, while for our system the ratio is the same (≈ 1) for both constituents. Though it appears that their calculation for collisions involving disparate particles is a bit different from ours, the different results may also be associated with the difference between their mixture (polydisperse) and ours (bidisperse). Our contact and kinetic stress partition coefficients are remarkably similar to those measured in DEM simulations of an inclined chute flow by Weinhart *et al.* (2013). In the form suggested by (5.3*a*) and (5.3*b*), we find for our mixture $b^c = 0$ and $b^k = -0.39$, while Weinhart *et al.* (2013) obtained values of $b^c = 0.02$ and $b^k = -0.38$.

Both Wiederseiner *et al.* (2011) (for experimental inclined chute flows) and Weinhart *et al.* (2013) (for simulated inclined chute flows) reported values for a maximum segregation velocity, $q = (b^c/c_D)g\cos\theta$ and b^c. Wiederseiner *et al.* (2011) reported values for q that ranged from $\approx 1.23 \times 10^{-3}$ to $\approx 1.99 \times 10^{-3}$ m s^{-1} that varied non-monotonically with shear rate. Weinhart *et al.* (2013) found for their simulations that q started with a maximum value of $\approx 6.8 \times 10^{-4}$ m s^{-1} and decreased to zero. Our maximum segregation velocity measured for our 50/50 mixture during the first half-second of rotation was $\approx 8.1 \times 10^{-4}$ m s^{-1}, similar to that of Weinhart *et al.* (2013), whose mixture was of the same size ratio of ours. The segregation velocity of Wiederseiner *et al.* (2011) was a bit higher, a result we might expect for their higher size ratio.

Our fitted results for c_D and d are also similar to published results for slightly different systems. Wiederseiner *et al.* (2011) measured values of $D = c_D/d$ for different conditions. Specifically, for an inclination of 29°, they reported finding that $D \equiv d/c_D$ ranges from 2.08 to 2.79×10^{-6} m^2 s^{-1}, a value which increased slightly with increasing shear rate. Using our fitted values for c_D and d, we obtain $D \approx 2 \times 10^{-6}$ m^2 s^{-1}, similar to those reported by Wiederseiner *et al.* (2011). We did not investigate shear rate dependence of our results, as we did not have sufficient data for clean predictions for this variation. On the other hand, our model contains an implicit dependence on shear rate via the dependence on kinetic stress gradient, e.g. in $\Phi^i_{\sigma k}$ in (2.11). Weinhart *et al.* (2013) presented temporal plots of both their segregation velocity, $q = (b^c/c_D)g\cos\theta$, and b^c, allowing us to calculate an approximate value of c_D to compare with our results. They showed that q started with a maximum value of $\approx 6.8 \times 10^{-4}$ m s^{-1} and decreased to zero, while b^c started with a maximum value of $b^c \approx 0.38$ and decreased to a relatively steady value of $b^c = 0.02$. Based on this, early time value of c_D was ≈ 8.58 s^{-1}, similar to but slightly larger than our approximate value of $c_D \approx 6.30$ s^{-1}.

Thornton *et al.* (2012) also performed chute flow experiments for binary mixtures with a range of size ratios. They investigated the dependence of segregation and diffusion on particle size ratio in a binary mixture. They reported their results in terms of a Péclet number Pe for segregation, which quantifies how large the segregation effects are compared to the diffusive effects: $Pe = qh/D$, where q is the maximum segregation velocity and $D = d/c_D$ as defined above, and h is a characteristic length. They found that the Péclet number increased linearly with

size ratio, and then plateaued at approximately 7.7. For a size ratio of 1.5, they estimated a range of $6 < Pe < 7.5$. Using the depth of dense flow of 15 mm as a characteristic length, the maximum depth-averaged normal velocity of 0.81 mm s^{-1}, and our value of $d/c_D \approx 2 \times 10^{-6}$ m^2 s^{-1}, the Péclet number for our simulation would be approximately 6.1 which is within the estimated range based on the work by Thornton *et al.* (2012).

7. Discussion: applicability to mixtures differing in size and density

The calculations in § 6 indicate that our model for segregation in gravity-driven dense flows is reasonable. However, there are still significant steps that need to be taken before the physics of the process is fully captured. In particular, model parameters such as stress partition coefficients, and the drag and diffusion coefficients are likely to vary with particle size and other particle properties such as density. So, while we believe that the model provides insight into the physics of the segregation process, particularly in identifying the importance of the kinetic stress gradient in segregating mixtures in a gravitational field, its applicability is limited until we find predictive forms for flow parameters.

Nevertheless, we consider the implications of this theoretical framework for predicting segregation in mixtures of particles differing in both size and density. As we discussed in the introduction, previous research has shown that in dense flows, when large particles are sufficiently denser than their smaller counterparts, the large particles will sink, rather than rise in the mixture. Here, we briefly look for signals of this reversal in key parameters in our theory. In particular, we consider a mixture with 90 % (by volume) small (2 mm) particles and 10 % large (3 mm) particles, where the large particles have a higher material density than the small particles ($\rho_M^L = 3.1\rho_M^S$). For this mixture, the segregation we report for our equal-density mixture is reversed (figure 12*a*).

Figure 12(*a*) shows a snapshot of the mixture after ≈30 s of rotation, by which time the segregation $S(t)$ has reached a constant value (as shown in figure 12*b*). The segregation evolution is very similar to those of the equal-density mixtures (e.g. figure 3, $\langle\phi^L\rangle = 0.1$). However in this case, the large denser particles do not move towards the top of the flowing layer; instead they sink to the bottom of the flowing layer and accumulate near the centre of rotation. This is reflected in figure 12(*c*) where there is a peak in solid fraction for the large, denser particles (and a corresponding trough for the small, less dense, particles) in the middle of the occupied portion of the drum. The mass fluxes in figure 12(*d*) (early times, ≈1 s into the simulation) show that for the majority of the flowing layer, the large, denser particles move downward, and the smaller denser particles move upward, a reversal of the 'Brazil-nut segregation' we report for our equal-density mixtures in this paper.

We include parametric plots of the stress partition coefficients in figure 12(*e*,*f*) equivalent to those in figures 5(*b*) and 5(*d*) (calculated at ≈30 s into the simulation). Similar to the results from the equal-density mixtures, the contact stress is partitioned between the constituents approximately as their local concentrations, and the kinetic stresses are not. However, in contrast to the results from the equal-density mixtures, the larger particles bear a higher portion of the kinetic stresses than their local concentration and the small particles bear a lower portion of the kinetic stresses than their local concentration. This reversal implies that the segregation contribution due to the kinetic stress gradient is now in the opposite direction to that in the equal-density cases.

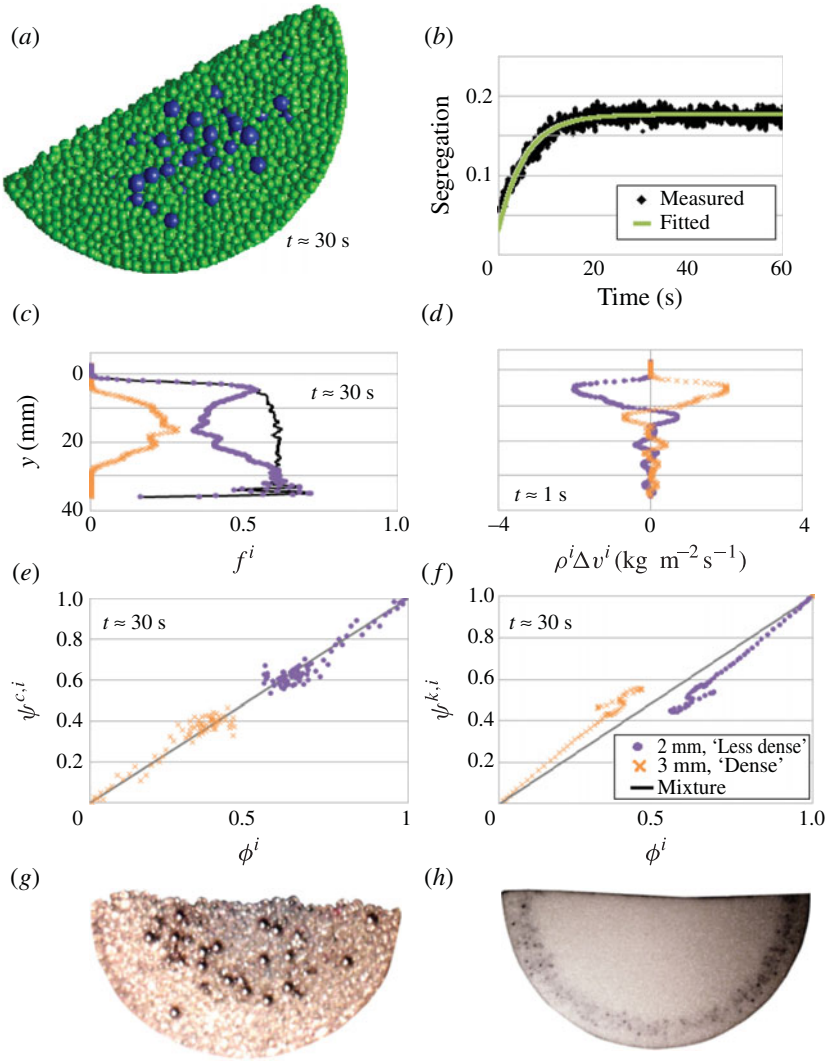

FIGURE 12. (Colour online) Segregation of a mixture with 90 % (by volume) small, less dense particles and 10 % large, denser ($\rho_M^L = 3.1\rho_M^S$) particles. (*a*) Snapshot of the mixture: segregation is reversed compared with figure 3. The segregation pattern is unfocused, possibly due to the relatively high diffusion compared with segregation 'driving forces'. (*b*) Segregation evolution: measured segregation $S(t)$ is calculated using (4.1) and fitted segregation $S^*(t)$ has the form of (4.2) with $S_f = 0.18$, $S_o = 0.11$, $t_d = 1.44$, and $\tau_c = 5.56$. (*c*) Solid fraction profile of both species and the mixture. (*d*) Initial segregation mass fluxes of the species as a function of depth. (*e*,*f*) Parametric plots of stress partition coefficients $\psi^{c,i}$ and $\psi^{k,i}$ as functions of local concentration ϕ^i. Plots (*c*–*f*) were obtained by averaging over 500 ms periods. (*g*) A photograph of intermediate segregation observed in a mixture of 2 mm glass (light) and 3 mm steel (dark) beads from our lab. Similar to the simulation in (*a*), the segregation of large particles is reversed; however the dense steel beads do not sink fully. (*h*) A photograph of intermediate segregation observed in a mixture of 3 mm (dark) and 0.5 mm (light) glass beads in a large drum (290 mm diameter) from our lab, where the larger beads do not rise fully to the top of the flowing layer.

A full analysis of these results requires more detailed consideration of the density variations in the mixture as segregation evolves (e.g. Fan & Hill 2014). Nevertheless, it is apparent that the difference between kinetic stress partitioning reverses, consistent with the reversal in the segregation behaviour observed in simulations (figure 12*a*) and experiments (figure 12*g*). In figure 12(*h*) we present an example of an experiment where denser larger particles segregate to an intermediate location in the drum. We are currently investigating whether or not a newer version of our theory allowing density variation captures this effect with a more systematic evaluation of model parameters. This could also enable a direct comparison with theories suitable for particles differing only in density such as that of Tripathi & Khakhar (2011, 2013).

Tripathi & Khakhar (2011, 2013) proposed a model for segregation of particles differing only in density for which they derived physics-based forms of the coefficients such as diffusion and drag, though the segregation mechanism is somewhat different. The segregation mechanism is one associated with effective buoyancy differences for particles in a mixture rather than kinetic sieving, though, interestingly, the segregation concentration evolution model is similar in form to the Gray–Thornton–Chugunov formulation apparent in (1.1). Essentially, for both model frameworks, the explicit dependence of the segregation term on constituent concentration is the same, and in both systems, segregation is driven by a pressure gradient associated with gravity. In the model by Tripathi & Khakhar (2011, 2013), drag and diffusion coefficients scale with a granular temperature, similar to a shear rate dependence that others have suggested for these variables for mixtures differing only in size. However, they do not include consideration of a more direct shear rate dependence – via temperature, kinetic stress, or otherwise – of segregation which we have shown to be important in this paper for particles differing only in size. We suspect, given the importance of buoyancy forces in mixtures of particles differing only in density, that pressure gradients associated with both gravity and kinetic stress gradients play explicit roles in segregating mixtures differing in both size and density. We are working on testing this conjecture with a newer version of our theory that allows for density variation (Fan & Hill 2014).

8. Conclusions

To summarize, we have developed a model for segregation that includes consideration of both kinetic stress gradient and gravity. We then used DEM simulations of gravity-driven flow in a drum to obtain stress partition coefficients for the mixture constituents. From these, we found that an explicit reference to gravity drops out. This suggests that gravity-driven kinetic sieving may not be active in these dense flows, but, instead, the kinetic stress gradient drives the segregation. Considering (5.2*a*,*b*) in (5.4), an equivalent form of (1.1*a*) for our model can be expressed by

$$\phi^i \left(v^i - v\right) = \phi^i \left(1 - \phi^i\right) A_k \frac{\mathrm{d}\sigma_{yy}^k}{\mathrm{d}y} + \left[-D\frac{\partial \phi^i}{\partial y}\right]. \tag{8.1}$$

Here, $A_k\ \mathrm{d}\sigma_{yy}^k/\mathrm{d}y$ replaces $A\ \mathrm{d}p/\mathrm{d}y$ in (1.1*a*) in the scaling of maximum segregation velocity. In other words, in contrast with recent models for segregation in dense flows, a gradient in kinetic stress (akin to granular temperature) is an important driving mechanism in our proposed model, while gravity plays primarily an implicit role by setting up the kinetic stress gradients associated with the shear rate gradient in the flow. In other words, even though kinetic stress (granular temperature) is

small, its gradient can be sufficiently large to drive segregation in dense flows. While the stress partition coefficients are based on empirical fits for one set of mixtures, we expect the form to be similar for other particle size ratios so that (8.1) holds for a wide range of mixtures, a conjecture we are currently testing with additional simulations.

In our dense flow simulations, we find that large particles of equal density to their smaller neighbours migrate to the top of the flowing layer primarily because this region corresponds to a region of higher kinetic stress and higher granular temperature. This segregation is driven in part by the manner in which contact stress and kinetic stress are partitioned among the species. The large particles bear a larger percentage of the contact stress than they do the kinetic stress, apparently pushing them away from the cooler regions. The smaller particles bear a larger percentage of the kinetic stress than they do the contact stress, allowing them to mobilize away from the high-temperature regions. While gravity does not appear explicitly in our final predictive form for the segregation dynamics, this does not imply that gravity does not play a role. Gravity, along with geometric considerations (Hill & Zhang 2008), drives the kinetic stress gradient. It may also play a role in the partitioning of the stresses, an issue we are currently investigating.

Additionally, we explored the effectiveness of a linear drag coefficient and diffusion parameter. We found that the linear form of these parameters is relatively effective and for this size ratio, the drag coefficient and diffusion parameter both vary minimally with concentration. Theoretical predictions using average values of both matched the measured segregation flux fairly well. Nonetheless it is valuable knowledge that variability with concentration exists, and this deserves further investigations.

This work is far from the first evidence of kinetic stress or granular temperature acting as a driving force in segregation. This dynamic features prominently in kinetic theory, which makes it informative to compare the prediction from our theory with segregation predicted by kinetic theory. Qualitatively, in systems correctly described by kinetic theory, the large particles are driven to the cooler region, in contrast with what we have found in dense systems (e.g. Xu *et al.* 2003; Galvin *et al.* 2005, Conway *et al.* 2006; Fan & Hill 2011*a*). Indeed, even recent attempts to expand kinetic theory to include structure appearing in denser systems predict that the larger particles move to cooler regions (e.g. Larcher & Jenkins 2013). We are currently developing a more quantitative comparison to understand the significance of these differences and the manner in which they appear in the modelling frameworks.

An appropriate model for the evolution of particle size distribution is critical for understanding a wide variety of flow behaviours in dense granular mixtures that depend on local particle size distribution. A relatively simple expression obtained recently for the rheology of dense granular flows (Pierre, Forterre & Pouliquen 2006; Forterre & Pouliquen 2008) applied to mixtures (Yohannes & Hill 2010; Tripathi & Khakhar 2011) demonstrates that the rheology depends on particle size distribution. The stresses generated by dense sheared granular flow itself also depend on particle size distribution (Hill & Yohannes 2011; Yohannes & Hill 2010). This, with the results in this paper indicating that internal stresses can drive segregation, suggests feedback mechanisms between particle size distribution and stresses that may drive some of the pattern formation and subsequent flow behaviours in simple and complex segregating systems that we are currently considering for modelling these flows.

Acknowledgements

We gratefully acknowledge funding for this research from NSF Grant No. CBET-0932735 and Proctor and Gamble. We are also grateful for helpful discussions with

Professors Jim Jenkins and Joe Goddard about segregation and rheology of dense systems, with Professors Stefan Luding, Thomas Weinhart, and Anthony Thornton about stress partitioning, and with Professor Randal Barnes for about error estimation in discrete deterministic systems.

REFERENCES

ABBOTT, J. R., TETLOW, N., GRAHAM, A. L., ALTOBELLI, S. A., FUKUSHIMA, E., MONDY, L. A. & STEPHENS, T. S. 1991 Experimental observations of particle migration in concentrated suspensions: Couette flow. *J. Rheol.* **35**, 773–795.

ALAM, M. & LUDING, S. 2003 Rheology of bidisperse granular mixtures via event-driven simulations. *J. Fluid Mech.* **276**, 69–103.

ALONSO, M., SATOH, M. & MIYANAMI, K. 1991 Optimum combination of size ratio, density ratio and concentration to minimize free surface segregation. *Powder Technol.* **68** (3), 145–152.

ARNARSON, B. Ö. & JENKINS, J. T. 2000 Particle segregation in the context of the species momentum balances. In *Traffic and Granular Flow '99: Social, Traffic and Granular Dynamics* (ed. D. Helbing, H. J. Herrmann, M. Schreckenberg & D. E. Wolf), pp. 481–487. Springer.

ARNARSON, B. Ö. & JENKINS, J. T. 2004 Binary mixtures of inelastic spheres: simplified constitutive theory. *Phys. Fluids* **16**, 4543–4550.

BATCHELOR, G. K. 1967 *An Introduction to Fluid Dynamics*. Cambridge University Press.

BONAMY, D., DAVIAUD, F. & LAURENT, L. 2002 Experimental study of granular surface flows via a fast camera: a continuous description. *Phys. Fluids* **15**, 1666–1674.

BRIDGWATER, J. 1976 Fundamental powder mixing mechanisms. *Powder Technol.* **15**, 215–231.

CAMPBELL, C. S. 2002 Granular shear flows at the elastic limit. *J. Fluid Mech.* **465**, 261–291.

CHIKKADI, V. & ALAM, M. 2009 Slip velocity and stresses in granular poiseuille flow via event-driven simulation. *Phys. Rev.* E **80**, 021303.

CONWAY, S. L., LIU, X. & GLASSER, B. J. 2006 Instability-induced clustering and segregation in high-shear couette flows of model granular materials. *Chem. Engng Sci.* **61**, 6404–6423.

CUNDALL, P. A. & STRACK, O. D. L. 1979 A discrete numerical model for granular assemblies. *Geotechnique* **29**, 47–65.

DIETRICH, W. E., KIRCHNER, J. W., IKEDA, H. & ISEYA, F. 1989 Sediment supply and the development of the coarse surface layer in gravel-bedded rivers. *Nature* **340**, 215–217.

DOLGUNIN, V. N. & UKOLOV, A. A. 1995 Segregation modeling of particle rapid gravity flow. *Powder Technol.* **83** (3), 95–103.

DONALD, M. B. & ROSEMAN, B. 1962 Mixing and de-mixing of solid particles: Part i. mechanisms in a horizontal drum mixer. *Brit. Chem. Engng* **7**, 749–752.

FAN, Y. & HILL, K. M. 2011*a* Phase transitions in shear-induced segregation of granular materials. *Phys. Rev. Lett.* **106**, 218301.

FAN, Y. & HILL, K. M. 2011*b* Theory for shear-induced segregation of dense granular mixtures. *New J. Phys.* **13**, 095009.

FAN, Y. & HILL, K. M. 2014 Shear-induced segregation of mixtures of particles differing in density. Under review.

FÉLIX, G. & THOMAS, N. 2004 Evidence of two effects in the size segregation process in dry granular media. *Phys. Rev.* E **70** (5), 051307.

FOO, W. S. & BRIDGWATER, J. 1983 Particle migration. *Powder Technol.* **36**, 271–273.

FORTERRE, Y. & POULIQUEN, O. 2008 Flows of dense granular media. *Annu. Rev. Fluid Mech.* **40**, 1–24.

GALVIN, J. E., DAHL, S. R. & HRENYA, C. M. 2005 On the role of non-equipartition in the dynamics of rapidly flowing, granular mixtures. *J. Fluid Mech.* **528**, 207–232.

GIOIA, G., OTT-MONSIVAIS, S. E. & HILL, K. M. 2006 Fluctuating velocity and momentum transfer in dense granular flows. *Phys. Rev. Lett.* **96**, 138001.

GRAY, J. M. N. T. & ANCEY, C. 2011 Multi-component particle-size segregation in shallow granular avalanches. *J. Fluid Mech.* **678**, 535–588.

GRAY, J. M. N. T. & CHUGUNOV, V. A. 2006 Particle-size segregation and diffusive remixing in shallow granular avalanches. *J. Fluid Mech.* **569**, 365–398.

GRAY, J. M. N. T. & THORNTON, A. R. 2005 A theory for particle size segregation in shallow granular free-surface flows. *Proc. R. Soc. Lond.* A **461**, 1447–1473.

HILL, K. M., CAPRIHAN, A. & KAKALIOS, J. 1997 Bulk segregation in rotated granular material measured by magnetic resonance imaging. *Phys. Rev. Lett.* **78**, 50–53.

HILL, K. M., DELLANGELO, L. & MEERSCHAERT, M. M. 2010*a* Heavy-tailed travel distance in gravel bed transport: an exploratory enquiry. *J. Geophys. Res.* **115**, F00A14.

HILL, K. M. & FAN, Y. 2008 Isolating segregation mechanisms in a split-bottom cell. *Phys. Rev. Lett.* **101**, 088001.

HILL, K. M., FAN, Y., ZHANG, J., VAN NIEKERK, C., ZASTROW, E., HAGNESS, S. C. & BERNHARD, J. T. 2010*b* Granular segregation studies for the development of a radar-based three-dimensional sensing system. *Granul. Matt.* **12**, 201–207.

HILL, K. M., GIOIA, G. & AMARAVADI, D. 2004 Radial segregation patterns in rotating granular mixtures: waviness selection. *Phys. Rev. Lett.* **93**, 224301.

HILL, K. M., GIOIA, G. & TOTA, T. 2003 Structure and kinematics in dense free-surface granular flow. *Phys. Rev. Lett.* **91**, 064302.

HILL, K. M., KHAKHAR, D. V., GILCHRIST, J. F., MCCARTHY, J. J. & OTTINO, J. M. 1999 Segregation-driven organization in chaotic granular flows. *Proc. Natl Acad. Sci. USA* **96**, 11701–11706.

HILL, K. M. & YOHANNES, B. 2011 Rheology of dense granular mixtures: boundary pressures. *Phys. Rev. Lett.* **106**, 058302.

HILL, K. M. & ZHANG, J. 2008 Kinematics of densely flowing granular mixtures. *Phys. Rev.* E **77**, 061303.

HSU, L., DIETRICH, W. E. & SKLAR, L. S. 2008 Experimental study of bedrock erosion by granular flows. *J. Geophys. Res.* **113**, F02001.

IDE, J. M. 1935 Comparison of statically and dynamically determined youngś modulus of rocks. *Proc. Natl Acad. Sci. USA* **22**, 81–92.

JAIN, N., OTTINO, J. M. & LUEPTOW, R. M. 2002 An experimental study of the flowing granular layer in a rotating tumbler. *Phys. Fluids* **14**, 572–582.

JAIN, N., OTTINO, J. M. & LUEPTOW, R. M. 2005 Combined size and density segregation and mixing in non-circular tumblers. *Phys. Rev.* E **71**, 051301.

JENKINS, J. T. & MANCINI, F. 1987 Balance laws and constitutive relations for plane flows of a dense, binary mixture of smooth, nearly elastic, circular disks. *Trans. ASME: J. Appl. Mech.* **54**, 27–34.

KHAKHAR, D. V., MCCARTHY, J. J. & OTTINO, J. M. 1997 Radial segregation of granular mixtures in rotating cylinders. *Phys. Fluids* **9**, 3600–3614.

KRISHNAN, G. P., BEIMFOHR, S. & LEIGHTON, D. T. 1996 Shear-induced radial segregation in bidisperse suspensions. *J. Fluid Mech.* **321**, 371–393.

KUHL, E., D'ADDETTA, G. A., HERRMANN, H. J. & RAMM, E. 2000 A comparison of discrete granular material models with continuous microplane formulations. *Granul. Matt.* **2** (5), 113–121.

LARCHER, M. & JENKINS, J. T. 2009*a* The influence of size segregation in particle-fluid flows. In *Powders and Grains 2009* (ed. M. Nakagawa & S. Luding), vol. 1145, pp. 1055–1058. American Institute of Physics.

LARCHER, M. & JENKINS, J. T. 2009*b* Size segregation in dry granular flows of binary mixtures. In *IUTAM-ISIMM Symposium on Mathematical Modeling and Physical Instances of Granular Flows* (ed. J. D. Goddard, J. T. Jenkins & P. Giovine), vol. 1227, pp. 363–370. American Institute of Physics.

LARCHER, M. & JENKINS, J. T. 2010 Particle size and density segregation in dense, dry granular flows. In *Proceedings of the First IAHR European Meeting, Edinburgh, UK*.

LARCHER, M. & JENKINS, J. T. 2013 Segregation and mixture profiles in dense, inclined flows of two types of spheres. *Phys. Fluids* **25**, 113301.

LEIGHTON, D. & ACRIVOS, A. 1987*a* Measurement of shear-induced self-diffusion in concentrated suspensions of spheres. *J. Fluid Mech.* **177**, 109–131.

LEIGHTON, D. & ACRIVOS, A. 1987*b* Shear-induced migration of particles in concentrated suspensions. *J. Fluid Mech.* **181**, 415–439.

MARKS, B. & EINAV, I. 2011 A cellular automaton for segregation during granular avalanches. *Granul. Matt.* **13**, 211–214.

MARKS, B., ROGNON, P. & EINAV, I. 2012 Grainsize dynamics of polydisperse granular segregation down inclined planes. *J. Fluid Mech.* **690**, 499–511.

MAY, L. B. H., GOLICK, L. A., PHILLIPS, K. C., SHEARER, M. & DANIELS, K. E. 2010*a* Shear-driven size segregation of granular materials: modeling and experiment. *Phys. Rev.* E **81**, 051301.

MAY, L. B. H., SHEARER, M. & DANIELS, K. E. 2010*b* Scalar conservation laws with nonconstant coefficients with application to particle size segregation in granular flows. *J. Nonlinear Sci.* **20**, 689–707.

MIDDLETON, G. V. & HAMPTON, M. A. 1976 Subaqueous sediment transport and deposition by sediment gravity flows. In *Marine Sediment Transport and Environmental Management* (ed. D. J. Stanley & D. J. P. Swift), pp. 197–218. John Wiley & Sons.

MORLAND, L. W. 1972 A simple constitutive theory for a fluid-saturated porous solid. *J. Geophys. Res.* **77**, 890–900.

MORLAND, L. W. 1978 A theory of slow fluid flow through a porous thermoelastic matrix. *Geophys. J. R. Astron. Soc.* **55**, 393–410.

MORLAND, L. W. 1992 Flow of viscous fluids through a porous deformable matrix. *Surv. Geophys.* **13**, 209–268.

NAYLOR, M. A. 1980 The origin of inverse grading in muddy debris flow deposits—a review. *J. Sedim. Petrol.* **50**, 1111–1116.

PAOLA, C. & SEAL, R. 1995 Grain size patchiness as a cause of selective deposition and downstream fining. *Water Resour. Res.* **31**, 1395–1407.

PIERRE, J., FORTERRE, Y. & POULIQUEN, O. 2006 A constitutive law for dense granular flows. *Nature* **441**, 727–730.

REDDY, K. A. & KUMARAN, V. 2010 Dense granular flow down an inclined plane: a comparison between the hard particle model and soft particle simulations. *Phys. Fluids* **22**, 113302.

SAVAGE, S. B. & LUN, C. K. K. 1988 Particle size segregation in inclined chute flow of dry cohesionless granular solids. *J. Fluid Mech.* **189**, 311–335.

SCHLICHTING, H. 1979 *Boundary-Layer Theory*. McGraw-Hill.

SHINBROT, T. & MUZZIO, F. 2000 Nonequilibrium patterns in granular mixing and segregation. *Phys. Today* **53** (3), 25–30.

SIMMONS, G. & BRACE, B. F. 1965 Comparison of static and dynamic measurements of compressibility of rocks. *J. Geophys. Res.* **70** (22), 5649–5656.

STEPHENS, D. J. & BRIDGWATER, J. 1978 The mixing and segregation of cohesionless particulate materials, part II. Microscopic mechanisms for particles differing in size. *Powder Technol.* **21**, 29–44.

STOCK, J. D. & DIETRICH, W. E. 2006 Erosion of steepland valleys by debris flows. *Geol. Soc. Am. Bull.* **118**, 1125–1148.

TABERLET, N., LOSERT, W. & RICHARD, P. 2004 Understanding the dynamics of segregation bands of simulated granular material in a rotating drum. *Europhys. Lett.* **68**, 522–528.

THORNTON, A., WEINHART, T., LUDING, S. & BOKHOVE, O. 2012 Modeling of particle size segregation: calibration using the discrete particle method. *Intl J. Mod. Phys.* C **23** (8), 1240014.

TRIPATHI, A. & KHAKHAR, D. V. 2011 Numerical simulation of the sedimentation of a sphere in a sheared granular fluid: a granular Stokes experiment. *Phys. Rev. Lett.* **107**, 108001.

TRIPATHI, A. & KHAKHAR, D. V. 2013 Density difference-driven segregation in a dense granular flow. *J. Fluid Mech.* **717**, 643–669.

TSUJI, Y., TANAKA, T. & ISHIDA, T. 1992 Lagrangian numerical simulation of plug flow of cohesionless particles in a horizontal pipe. *Powder Technol.* **71**, 239–250.

WEINHART, T., LUDING, S. & THORNTON, A. R. 2013 From discrete particles to continuum fields in mixtures. In *Powders and Grains 2011*, vol. 1542, pp. 1202–1205. American Institute of Physics.

WEINHART, T., THORNTON, A. R., LUDING, S. & BOKHOVE, O. 2012 From discrete particles to continuum fields near a boundary. *Granul. Matt.* **14** (2), 289–294.

WIEDERSEINER, S., ANDREINI, N., ÉPELY-CHAUVIN, G., MOSER, G., MONNEREAU, M., GRAY, J. M. N. T. & ANCEY, C. 2011 Experimental investigation into segregating granular flows down chutes. *Phys. Fluids* **23**, 013301.

WILLIAMS, J. C. 1963 The segregation of powders and granular materials. *Powder Technol.* **14**, 29–34.

WILLIAMS, J. C. 1976 The segregation of particulate materials. *Powder Technol.* **15**, 245–256.

XU, H., LOUGE, M. & REEVES, A. 2003 Solutions of the kinetic theory for bounded collisional granular flows. *Contin. Mech. Thermodyn.* **15**, 321–349.

YOHANNES, B. & HILL, K. M. 2010 Rheology of dense granular mixtures: particle-size distributions, boundary conditions, and collisional time scales. *Phys. Rev.* E **82**, 061301.

YOHANNES, B., HSU, L., DIETRICH, W. E. & HILL, K. M. 2010 Boundary stresses due to impacts from dry granular flows. *J. Geophys. Res.* **117**, F02027.